



# Isoprene and monoterpene simulations using the chemistry–climate model EMAC (v2.55) with interactive vegetation from LPJ-GUESS (v4.0)

Ryan Vella<sup>1,2</sup>, Matthew Forrest<sup>3</sup>, Jos Lelieveld<sup>1,4</sup>, and Holger Tost<sup>2</sup>

<sup>1</sup>Atmospheric Chemistry Department, Max Planck Institute for Chemistry, Mainz, Germany

<sup>2</sup>Institute for Atmospheric Physics, Johannes Gutenberg University Mainz, Mainz, Germany

<sup>3</sup>Senckenberg Biodiversity and Climate Research Centre (SBiK-F), Frankfurt am Main, Germany

<sup>4</sup>Climate and Atmosphere Research Center, The Cyprus Institute, Nicosia, Cyprus

**Correspondence:** Ryan Vella (ryan.vella@mpic.de) and Holger Tost (tosth@uni-mainz.de)

Received: 10 June 2022 – Discussion started: 1 July 2022

Revised: 28 December 2022 – Accepted: 14 January 2023 – Published: 3 February 2023

**Abstract.** Earth system models (ESMs) integrate previously separate models of the ocean, atmosphere and vegetation into one comprehensive modelling system enabling the investigation of interactions between different components of the Earth system. Global isoprene and monoterpene emissions from terrestrial vegetation, which represent the most important source of volatile organic compounds (VOCs) in the Earth system, need to be included in global and regional chemical transport models given their major chemical impacts on the atmosphere. Due to the feedback of vegetation activity involving interactions with weather and climate, a coupled modelling system between vegetation and atmospheric chemistry is recommended to address the fate of biogenic volatile organic compounds (BVOCs). In this work, further development in linking LPJ-GUESS, a global dynamic vegetation model, to the atmospheric-chemistry-enabled atmosphere–ocean general circulation model EMAC is presented. New parameterisations are included to calculate the foliar density and leaf area density (LAD) distribution from LPJ-GUESS information. The new vegetation parameters are combined with existing LPJ-GUESS output (i.e. leaf area index and cover fractions) and used in empirically based BVOC modules in EMAC. Estimates of terrestrial BVOC emissions from EMAC's submodels ONEMIS and MEGAN are evaluated using (1) prescribed climatological vegetation boundary conditions at the land–atmosphere interface and (2) dynamic vegetation states calculated in LPJ-GUESS (replacing the “offline” vegetation inputs). LPJ-GUESS-driven global emission estimates for isoprene and monoterpenes

from the submodel ONEMIS were 546 and 102 Tg yr<sup>−1</sup>, respectively. MEGAN determines 657 and 55 Tg of isoprene and monoterpene emissions annually. The new vegetation-sensitive BVOC fluxes in EMAC are in good agreement with emissions from the semi-process-based module in LPJ-GUESS. The new coupled system is used to evaluate the temperature and vegetation sensitivity of BVOC fluxes in doubling CO<sub>2</sub> scenarios. This work provides evidence that the new coupled model yields suitable estimates for global BVOC emissions that are responsive to vegetation dynamics. It is concluded that the proposed model set-up is useful for studying land–biosphere–atmosphere interactions in the Earth system.

## 1 Introduction

The land surface of the Earth is dominated by vegetation, with forests covering  $\sim 42 \times 10^6$  km<sup>2</sup> in tropical, temperate and boreal regions, making up  $\sim 30\%$  of the total land area (Bonan, 2008). The terrestrial biosphere is known to be a primary source of volatile organic compounds (VOCs) such as isoprene and various terpenes, accounting for around 90 % of the total VOC emissions to the atmosphere (Guenther et al., 1995). The processes driving VOC emissions from plants are complex and not fully understood; however, biogenic volatile organic compounds (BVOCs) seem to play a role in protecting photosynthetic activity in plants from damage caused by

reactive oxygen species, which are synthesised in leaves at high temperatures (Niinemets, 2010; Harrison et al., 2013; Lantz et al., 2019). BVOC emissions can also be triggered by other chemical, physical or biological stresses and processes, e.g. herbivory (Laothawornkitkul et al., 2008), signalling between organisms (Zuo et al., 2019) or also oxidative stress originating from the atmosphere (e.g. under elevated ozone concentrations; Sharkey et al., 2008). Plants emit an array of VOCs, but different plant species emit different compounds according to their evolutionary adaptation. For example, the emission of isoprene can be considered an evolutionary trait that benefits certain plant species in hot, dry environments (Taylor et al., 2018). Isoprene and monoterpenes are the most abundant species among the BVOCs (Kesselmeier and Staudt, 1999; Lathiere et al., 2006; Guenther et al., 2012), and their high reactivity exerts a significant influence on atmospheric composition (Atkinson, 2000). The atmospheric chemical lifetime of such BVOCs ranges from minutes to hours (Atkinson and Arey, 2003), as they quickly interact with tropospheric species including carbon monoxide, hydroxyl radicals and ozone (Lelieveld et al., 1998; Granier et al., 2000; Poisson et al., 2000; Pfister et al., 2008), thus altering the atmosphere's oxidation capacity. BVOCs are also the primary precursor for secondary organic aerosols (SOAs), which can exert a significant forcing on the radiative balance of Earth, both directly through scattering and absorption of solar radiation and indirectly through changing cloud properties (Rap et al., 2013; Scott et al., 2014). SOA also contributes to changes in the radiation balance by decreasing the solar near-surface direct radiation while at the same time increasing the diffusive radiation contribution (Wang et al., 2019).

The first BVOC models employed empirical relations describing the isoprene emission rate dependencies on temperature and light (Guenther et al., 1991, 1993; Tingey et al., 1981) and monoterpene emission rate dependency on temperature (Evans et al., 1982; Lamb et al., 1987; Tingey et al., 1980, 1981). The formulations include a species- or vegetation-type-specific emission factor characterised from field or laboratory measurements (e.g. Lamb et al., 1985; Arey et al., 1991; Guenther et al., 1993) which is defined for arbitrarily chosen environmental conditions (usually 30 °C and 1000  $\mu\text{mol photons per metre squared per second}$ ; Grote and Niinemets, 2007). This approach has been extensively used to study different ecosystem types all over the world, including deserts (Geron et al., 2006), grassland (Bai et al., 2006), savanna (Guenther et al., 1999; Otter et al., 2003), Mediterranean (Cortinovis et al., 2005), tropical (Harley et al., 2004), temperate (Karl et al., 2003) and boreal forests (Westberg et al., 2000). Empirical algorithms are also presently used in well-established global BVOC models such as ONEMIS (Kerkweg et al., 2006) and MEGAN (Guenther et al., 2006). These modules are presently integrated into the modelling system considered in this study (EMAC).

The land–biosphere–atmosphere interface in models is fundamentally important for studying the fate of BVOCs in the atmosphere; yet, early models were designed to simulate single components of the Earth system in isolation, prescribing simple, non-interacting boundary conditions at the interface. However, models have become increasingly coupled, with dynamic multidirectional fluxes between the different models considered. This has yielded a new category of models that we now call Earth system models (ESMs). ESMs are highly comprehensive tools ideal for modelling past and future climate change with biogeochemical feedbacks and also for studying biosphere–atmosphere interactions explicitly (Flato et al., 2014). To this end, several modelling studies have linked atmospheric-chemistry-enabled models with dynamic vegetation models to investigate the impacts of changing vegetation cover on global atmospheric emissions, atmospheric chemistry and future climate change (e.g. Levis et al., 2003; Sanderson et al., 2003; Naik et al., 2004; Lathiere et al., 2005; Arneth et al., 2007b).

Sporre et al. (2019) employed an ESM to investigate climate forcing caused by BVOC–aerosol feedbacks, where it was determined that increased BVOC emissions and subsequent SOA formation in future climate scenarios result in  $-0.43 \text{ W m}^{-2}$  stronger net cloud forcing and  $-0.06 \text{ W m}^{-2}$  forcing from the direct scattering of sunlight. A new ESM that integrates the chemistry–climate model EMAC (Roegner et al., 2006; Jöckel et al., 2005) with the dynamic global vegetation model (DGVM) LPJ-GUESS (Smith et al., 2001; Sitch et al., 2003; Smith et al., 2014) has recently been developed (Forrest et al., 2020). In a first study, the coupled model gave a good representation of worldwide potential natural vegetation distribution, despite some regional variations, especially at lower spatial resolutions. This study presents further model coupling of LPJ-GUESS within the EMAC modelling system with respect to vegetation-driven emissions. New vegetation parameters are computed from LPJ-GUESS variables and used as (online) input vegetation information for empirically based BVOC modules (ONEMIS and MEGAN) in EMAC. The new vegetation-sensitive isoprene and monoterpene emission fluxes in EMAC are evaluated and compared against emissions from the semi-process-based module (Niinemets et al., 2002, 1999) in LPJ-GUESS. The new model configuration is then used to examine temperature and fertilisation effects in doubling  $\text{CO}_2$  climate scenarios.

## 2 Methods

### 2.1 EMAC modelling system (v2.55)

The EMAC (ECHAM/MESSy Atmospheric Chemistry) model is a numerical chemistry and climate modelling system that includes submodels that describe tropospheric and middle atmosphere processes, in addition to their interac-

tions with oceans, land and anthropogenic activities. It originally combined the ECHAM atmospheric general circulation model (GCM; Roeckner et al., 2006) with the Modular Earth Submodel System (MESSy; Jöckel et al., 2005) framework and philosophy, where physical processes and most of the infrastructure has been divided into “modules”, which can be further developed to improve existing process representations, and new modules can be added to represent new or alternative process representations. EMAC has been further developed to include a broader representation of atmospheric chemistry by coupling different processes such as representations for aerosols, aerosol–radiation and aerosol–cloud interactions (e.g. Tost, 2017). In this study, version 2.55 has been utilised, which is based on the well-documented version used in comprehensive model intercomparison studies (e.g. Jöckel et al., 2016).

### BVOC modules in EMAC

Both ONEMIS and MEGAN are emission modules which are based on the Guenther algorithms (Guenther et al., 1993, 1995), where emissions are calculated as a function of ecosystem-specific emission factors, surface radiation, temperature, the foliar density and its vertical distribution. The schemes mostly differ in the evaluation of the canopy process for light and temperature sensitivity on emission yields. In ONEMIS, fluxes are a function of foliar density, plant-specific emission factors and an activity factor accounting for light and temperature sensitivity. Emissions are calculated within four distinguished layers of the canopy, expressed by the leaf area density (LAD) and leaf area index (LAI). For each layer, the extinction of photosynthetically active radiation (PAR) is calculated from the direct, visible radiation and the zenith angle. The fractions of sunlit leaves and the total biomass are then used to calculate emissions from sunlit and shaded leaves within the canopy. On the other hand, fluxes in MEGAN are a function of the LAI, plant-specific emission factors, light, temperature and wind conditions within the canopy, leaf age and soil moisture. In MEGAN, the parameterised canopy environment emission activity (PCEEA) algorithm is used rather than the alternative detailed canopy environment model that calculates light and temperature at each canopy depth. The PCEEA algorithm calculates the light sensitivity within the canopy as a function of the daily average above-canopy photosynthetic photon flux density (PPFD), the solar angle and a non-dimensional factor describing the PPFD transmission through the canopy. Further technical details for canopy processes employed in ONEMIS can be found in Ganzeveld et al. (2002), while Guenther et al. (2006) provide details for MEGAN.

### 2.2 LPJ-GUESS DGVM (v4.0)

The following section is based on the standard copyright-free LPJ-GUESS model description template ([https://web.nateko.](https://web.nateko.lu.se/lpj-guess/resources.html)

[lu.se/lpj-guess/resources.html](https://web.nateko.lu.se/lpj-guess/resources.html), last access: 14 January 2023). The Lund-Potsdam-Jena General Ecosystem Simulator (LPJ-GUESS; Smith et al., 2001; Sitch et al., 2003; Smith et al., 2014) is a DGVM featuring an individual-based model of vegetation dynamics. These dynamics are simulated as the emergent outcome of growth and competition for light, space and soil resources among woody plant individuals and a herbaceous understorey in each of a number (50 in this study) of replicate patches representing random samples of each simulated locality or grid cell. The simulated plants are classified into 1 of 12 plant functional types (PFTs) discriminated by growth form, phenology, photosynthetic pathway ( $C_3$  or  $C_4$ ), bioclimatic limits for establishment and survival and, for woody PFTs, allometry and life history strategy. LPJ-GUESS has already been implemented in global ESMs (e.g. Weiss et al., 2014; Alessandri et al., 2017), and more recently coupled with EMAC (Forrest et al., 2020). LPJ-GUESS coupled with EMAC currently provides information on potential natural vegetation rather than present-day vegetation; hence, the current configuration cannot be validated yet. However, land use configurations are currently included in the coupled EMAC/LPJ-GUESS system, allowing for a more realistic representation of the vegetation dynamics in upcoming studies.

### BVOC emission routine in LPJ-GUESS

LPJ-GUESS includes a built-in BVOC emission module for the calculation of isoprene and monoterpene emission fluxes. The submodel combines the process-based leaf-level emission model (Niinemets et al., 2002, 1999), which is also based on the Guenther algorithms, with the LPJ-GUESS vegetation model for isoprene (Arneth et al., 2007b) and monoterpene (Schurgers et al., 2009) emissions. The algorithm computes BVOC production based on photosynthetic electron flux, emission factors, temperature, seasonality and also includes a  $CO_2$  inhibition factor on leaf production of isoprene and monoterpenes relative to the  $\sim 370$  ppmv (parts per million by volume)  $[CO_2]$  in the year 2000. Further technical details on the algorithm can be found in Hantson et al. (2017).

The algorithm also needs the daily temperature range (DTR) for the calculation of BVOC emission rates, which are typically derived from climatological datasets. In this study, the DTR (defined as the difference between the maximum and minimum daily temperature) is computed in EMAC and is passed on to LPJ-GUESS on a daily basis.

Semi-process-based BVOC emissions from the LPJ-GUESS module are only calculated within the LPJ-GUESS model part and are not integrated into or transferred to EMAC at the current stage. This also means that such emissions are only available as daily averages, in contrast to the emissions provided by ONEMIS and MEGAN in EMAC, which exhibit a diurnal cycle. Thus, having LPJ-GUESS-driven emissions from ONEMIS and MEGAN in EMAC pro-

vides more consistency, including the direct link between weather, climate (change) and the impacts on vegetation and, hence, emissions. An adaptation of this LPJ-GUESS module to the shorter (a few minutes) time step of EMAC is rather complicated, especially when the current scheme uses daily average light fluxes and a daily temperature range instead of individual snapshots of radiative fluxes and temperature. This would require a complete retuning of the emission scheme, with the only benefit being the higher temporal resolution of the emission fluxes (which cannot be utilised in LPJ-GUESS but only in EMAC). Even though the scheme of Niinemets et al. (1999) is semi-process based, the processes are also highly parameterised, such that the advantages against the Guenther et al. (1993, 1995) algorithms are also small. In this work, BVOC emissions from the LPJ-GUESS routine are used for comparison only.

### 2.3 LPJ-GUESS-EMAC coupling for BVOC emission estimates

#### 2.3.1 Overview of the coupling between EMAC and LPJ-GUESS

This study is part of a roadmap in which the model integration between EMAC and LPJ-GUESS is gradually tightened in well-defined, consecutive steps. To clarify the significance of this work, the roadmap from Forrest et al. (2020) is reproduced (Fig. 1), and the modelling development and evaluation efforts in this study are highlighted. This study focuses on BVOC model processes in EMAC based on interactive vegetation from LPJ-GUESS. It extends the model coupling between EMAC and LPJ-GUESS in Forrest et al. (2020) by employing new parameterisations to calculate the foliar density and leaf area density distribution from vegetation states in LPJ-GUESS. The new parameters from LPJ-GUESS are combined with existing ones (e.g. LAI and cover fractions) and are used to run empirically based BVOC modules in EMAC (i.e. ONEMIS and MEGAN). The semi-process-based BVOC emissions from LPJ-GUESS are not integrated into EMAC and are only evaluated against the new vegetation-sensitive empirically based emissions fluxes in EMAC.

#### 2.3.2 Simulation set-up

In this work, the coupling strategy employed in Forrest et al. (2020) is employed, where modifications are done in LPJ-GUESS, such that it provides its functionality (i.e. vegetation information) via a new submodel in the MESSy framework, yet keeping the LPJ-GUESS source code intact with minimal modification. At a regular interval (currently 24 h at 12:00 UTC) EMAC provides LPJ-GUESS with the daily mean 2 m temperature, daily mean net downwards shortwave radiation and the total daily precipitation. Daily CO<sub>2</sub> concentrations and nitrogen deposition are also transferred from

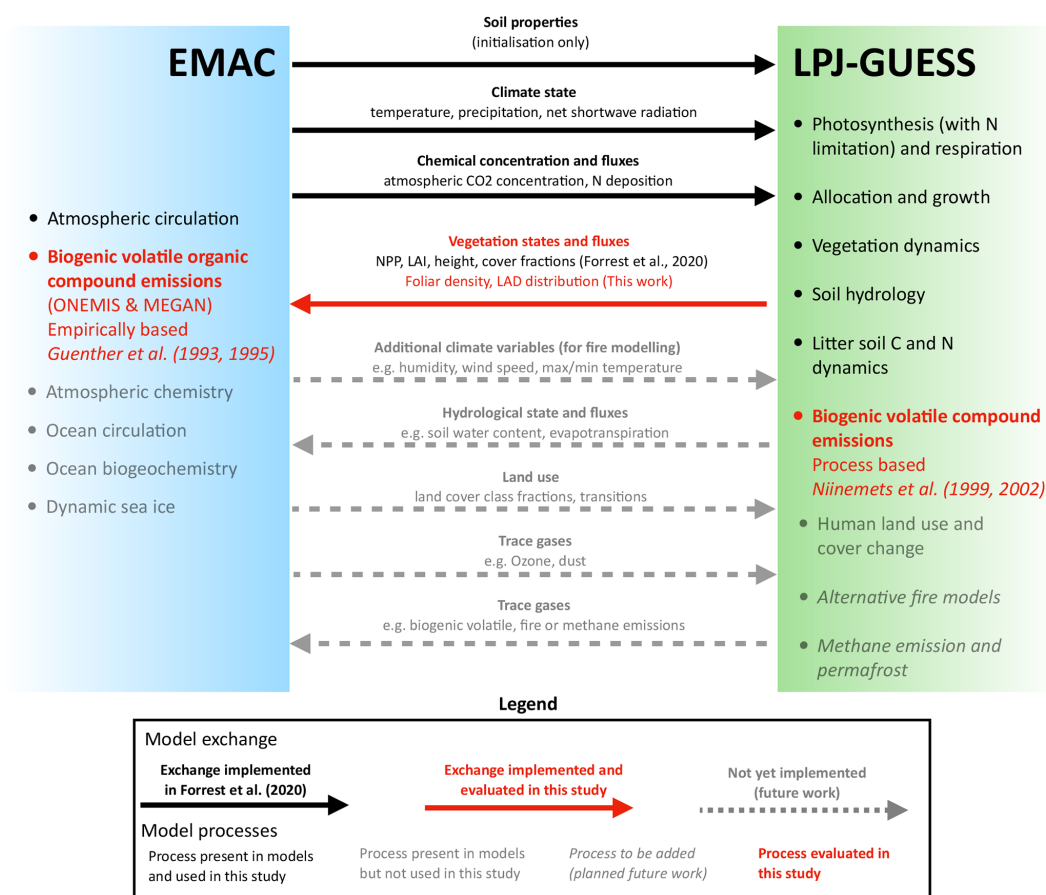
EMAC to LPJ-GUESS. As a result, the LPJ-GUESS land surface conditions are entirely determined by the EMAC atmospheric state and chemical fluxes. In Forrest et al. (2020), only one-way coupling was performed (see Fig. 1), which means that LPJ-GUESS calculations are entirely based on EMAC information; however, the land surface vegetation condition calculated in LPJ-GUESS has no effect on the atmospheric state in EMAC. In this study, existing LPJ-GUESS output variables (i.e. LAI and PFT fractional coverage) are utilised to calculate isoprene and monoterpene emission rates in EMAC, allowing, for the first time, dynamic vegetation information from LPJ-GUESS to be passed back to EMAC and used for BVOC fluxes calculations in ONEMIS and MEGAN. Note that the hydrological cycle uses the ECHAM5 native soil moisture, and the hydrological information from LPJ-GUESS does not feed back to the meteorology. Similarly, plant albedo and roughness height are not allowed to influence the meteorology either, but climatological values are used to drive the weather and climate conditions of EMAC in the applied model configuration, even though these links are also implemented and pending throughout the evaluation.

Figure 2 illustrates the model configuration for computing isoprene and monoterpene emissions fluxes in EMAC using the submodels of ONEMIS and MEGAN. Both models require emission factors for the various PFTs, the solar zenith angle, surface radiation and surface temperature. Additionally, ONEMIS requires the following vegetation variables: leaf area index (LAI), foliar density and leaf area density (LAD) canopy profile. In contrast, MEGAN requires the LAI and fractional coverage of broadleaf, needleleaf, grass and shrub ecosystem types. In the original set-up, the vegetation input variables are prescribed from offline climatological datasets, whereas, in the new configuration, the climatological vegetation variables are replaced with ones calculated online in LPJ-GUESS. This implies that the new set-up feeds dynamic vegetation states to the BVOC modules that are directly computed in LPJ-GUESS on a daily timescale and driven by atmospheric states and chemical fluxes in EMAC, allowing for estimates of isoprene and monoterpene emissions with dynamic vegetation. The coupling is performed from the EMAC side by implementing new calculations using LPJ-GUESS information to derive all vegetation variables needed in ONEMIS and MEGAN for the computation of BVOC emission fluxes. Details on the vegetation variables required in ONEMIS and MEGAN, in addition to the new parameterisations used for their calculation, are described in the next section.

#### 2.3.3 Vegetation variables for the BVOC modules

- *Leaf area index.* Measurements of the number of leaves in the canopy are required for ecosystem studies such as this one. This metric is often defined as the leaf area index (LAI), which is the one-sided leaf area in the





**Figure 1.** The main processes and exchanges in the coupled model framework adopted from Forrest et al. (2020). Model exchanges in normal black text were included in Forrest et al. (2020) and used in the simulations presented here. Exchanges in red are implemented in this work, while exchanges with grey text and grey dotted arrows are not currently included in the framework but are planned for use in future work. Model processes in normal black text were included in Forrest et al. (2020). Processes in normal grey text were included in Forrest et al. (2020) but not used here, while processes in italicised grey text are not currently included in the framework. Processes in red on the EMAC side (empirically based emissions with interactive vegetation information) are implemented and evaluated in this work, while BVOC emissions in LPJ-GUESS (semi-process based) were already implemented and are only used in this study for comparison with EMAC emissions.

canopy per unit surface area of the ground ( $\text{m}^2 \text{m}^{-2}$  Jordan, 1969). In DGVMs, including LPJ-GUESS, this is a standard output variable.

- *Foliar density.* The foliar density  $D$  (grams of dry matter in metres squared), sometimes referred to as dry matter (DM), can be derived directly from the LAI as follows (Guenther et al., 1995):

$$D = \text{LAI} \cdot S_{\text{LW}}, \quad (1)$$

where  $S_{\text{LW}}$  is an average specific leaf weight ( $\text{g m}^{-2}$ ) and is given for each ecosystem (or PFT) based on Box (1981).

- *Leaf area density distribution.* The leaf area density (LAD) is a metric describing the leaf area in a cubic volume within the canopy ( $\text{m}^2 \text{m}^{-3}$ ). The original

ONEMIS configuration employs an expert-driven offline dataset from a dry deposition inferential model (DDIM; Weiss and Norman, 1985) to characterise the LAD distribution for the following three types of vegetation: (i) agricultural crops, (ii) deciduous forests and (iii) coniferous forests. The 12 PFTs (used in the applied LPJ-GUESS set-up) were classified into these three groups, with grass PFTs included in the “agricultural crop” category. The LAD distribution for each of the vegetation types is divided into four equal layers, i.e. LAD 1 (top layer), LAD 2, LAD 3 and LAD 4 (bottom layer).

These values are then used in ONEMIS for calculating the photosynthetic active radiation (PAR) within the canopy and subsequent BVOC emission estimates. For the LPJ-GUESS output, a parameterisation derived

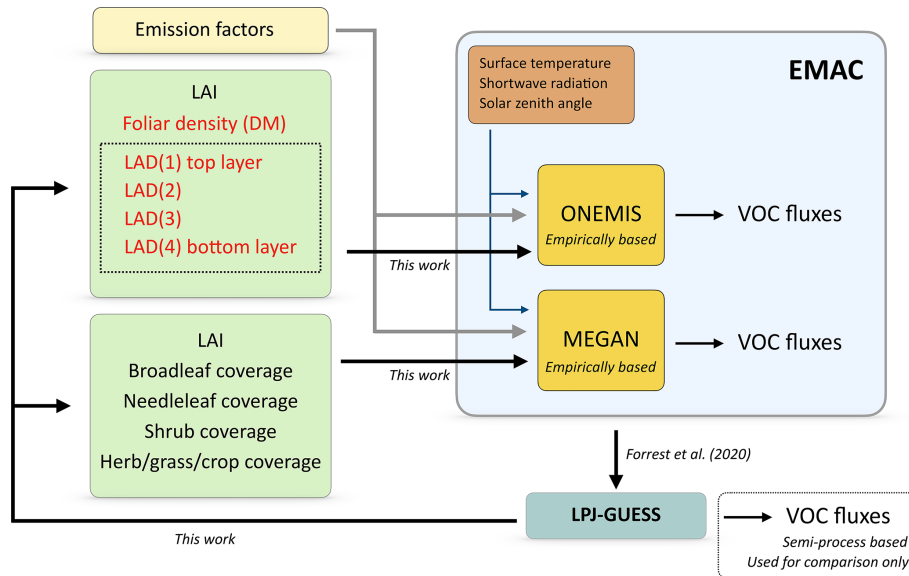


**Figure 2.** Model set-up for BVOC emission estimates in EMAC. The vegetation variables needed in ONEMIS and MEGAN are now provided by LPJ-GUESS, replacing offline climatological datasets. Vegetation variables that were already available at the interface between EMAC and LPJ-GUESS are in normal black text, while the new vegetation information derived in this work (i.e. foliar density and the LAD distribution) are in red text. Note that, in EMAC, only empirically based emissions are considered. VOC fluxes from the semi-process-based module in LPJ-GUESS are only used for comparison.

by Lalic et al. (2013) is employed to compute similar LADs at four canopy levels in the interface submodel between EMAC and LPJ-GUESS. The empirical relation describes the LAD at a height  $z$  (in m) as a function of the maximum LAD ( $LAD_{\max}$ ), the canopy height  $h$  and the height  $z_m$  corresponding to  $LAD_{\max}$  (see Fig. 3).

$$LAD(z) = LAD_{\max} \left( \frac{h - z_m}{h - z} \right)^n \times \exp \left[ n \left( 1 - \frac{h - z_m}{h - z} \right) \right] \quad \begin{matrix} n = 6 & \text{for } 0 \leq z < z_m \\ n = \frac{1}{2} & \text{for } z_m \leq z \leq h. \end{matrix} \quad (2)$$

First, the ratio between the canopy height ( $h$ ) and the height corresponding to  $LAD_{\max}$  (i.e.  $h/z_m$ ) for each vegetation class using LAD canopy profiles from the DDIM is determined. The dataset has 21 layers, and the layer where  $LAD_{\max}$  occurs ( $z_m$ ) is utilised to compute  $h/z_m$  as follows:

- i. Agricultural crops, with  $z_m/h = 12/21 \approx 0.57$ .
- ii. Deciduous forests, with  $z_m/h = 15/21 \approx 0.71$ .
- iii. Coniferous forests, with  $z_m/h = 17/21 \approx 0.81$ .

$LAD_{\max}$  for each PFT is calculated from the corresponding LAI and PFT height  $h$  information from LPJ-GUESS, in addition to the ratio  $h/z_m$ , given the follow-

ing relation:

$$LAI = \int_0^h LAD = \int_0^h LAD_{\max} \left( \frac{h - z_m}{h - z} \right)^n \times \exp \left[ n \left( 1 - \frac{h - z_m}{h - z} \right) \right] dz. \quad (3)$$

After a numerical value for  $LAD_{\max}$  for each PFT is computed, the LAD at four canopy layers is calculated via Eq. (2) by integrating over four equal layers within the total canopy height  $h_{\text{tot}}$ . In all set-ups used in the study, the total canopy height  $h_{\text{tot}}$  is assumed to have a value of 25 m. This results in the following:

$$\begin{aligned} LAD(1) &= \int_{0.75h_{\text{tot}}}^{h_{\text{tot}}} LAD_{\max} \left( \frac{h - z_m}{h - z} \right)^n \times \exp \left[ n \left( 1 - \frac{h - z_m}{h - z} \right) \right] dz, \\ LAD(2) &= \int_{0.5h_{\text{tot}}}^{0.75h_{\text{tot}}} LAD_{\max} \left( \frac{h - z_m}{h - z} \right)^n \times \exp \left[ n \left( 1 - \frac{h - z_m}{h - z} \right) \right] dz, \\ LAD(3) &= \int_{0.25h_{\text{tot}}}^{0.5h_{\text{tot}}} LAD_{\max} \left( \frac{h - z_m}{h - z} \right)^n \times \exp \left[ n \left( 1 - \frac{h - z_m}{h - z} \right) \right] dz, \end{aligned}$$

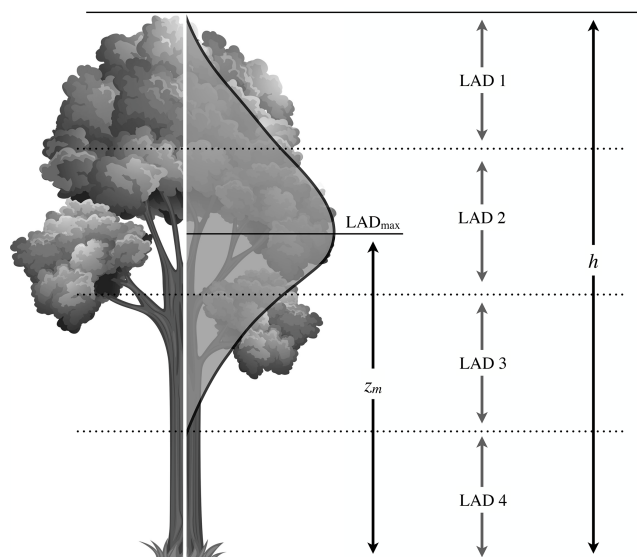


**Figure 3.** Graphical representation of the canopy LAD distribution.  $LAD_{\max}$  is the maximum LAD within the canopy,  $z_m$  is the height from the ground at which  $LAD_{\max}$  occurs, and  $h$  is the total canopy height. LAD 1, LAD 2, LAD 3 and LAD 4 are four equal canopy layers.

$$LAD(4) = \int_0^{0.25h_{\text{tot}}} LAD_{\max} \left( \frac{h - z_m}{h - z} \right)^n \times \exp \left[ n \left( 1 - \frac{h - z_m}{h - z} \right) \right] dz, \quad (4)$$

where  $z_m$  is a fraction of  $h$  based on the PFT vegetation classes i, ii or iii, and  $h$  is the PFT height. Figure 4 compares the LAD distribution from DDIM point data, used in the previous set-up, with the new parameterisation described in Eq. (2).

- *Vegetation class coverage.* The vegetation coverage refers to the fraction of land area occupied by certain PFTs in one grid cell. This variable is used in MEGAN to adjust emission rates from different vegetation classes. This variable is already calculated in LPJ-GUESS for each of the 12 PFTs.

## 2.4 Set-up for double CO<sub>2</sub> scenarios

The submodel RAD in EMAC (Dietmüller et al., 2016) simulates the radiative transfer in the atmosphere accounting for the effects of the shortwave and longwave radiation fluxes from radiatively active trace gases. CO<sub>2</sub> has the largest radiative influence in the longwave range of the spectrum, resulting in radiative forcings leading to stratospheric cooling and tropospheric warming. The CO<sub>2</sub> value prescribed in

RAD mainly dictates the surface temperatures resulting from the greenhouse effect, while CO<sub>2</sub> in the vegetation scheme (i.e. in LPJ-GUESS) determines the carbon available for photosynthesis and, hence, accounts for CO<sub>2</sub> fertilisation effects.

Climatological monthly average sea surface temperature (SST) and sea ice content (SIC) from the Atmospheric Model Intercomparison Project (AMIP) database from 1987 to 2006 are used for Ref and Bio × 2, with a prescribed CO<sub>2</sub> of 348 ppmv in the radiation scheme. However, with 696 ppmv [CO<sub>2</sub>] in the radiation scheme (i.e. in Atm × 2 and Both × 2), oceanic boundary conditions are prescribed using external data corresponding to SST and SIC at 696 ppmv to preserve radiative equilibrium. These data are acquired from a coupled atmosphere–ocean general circulation model (increased/decreased SSTs/SICs) performed under identical climate circumstances (696 ppmv [CO<sub>2</sub>]; same approach as in Rybka and Tost, 2014).

## 3 Results and discussion

### 3.1 Vegetation characteristics as input to the emission routines

In this section, the LPJ-GUESS state variables needed as input for the BVOC routines are discussed. For that purpose, the LPJ-GUESS output is compared with the corresponding offline climatological datasets used for BVOC emission estimates in ONEMIS and MEGAN in the original model configuration i.e. with prescribed vegetation boundary conditions. For such comparisons, it has to be kept in mind that the neglect of land use in LPJ-GUESS means that currently only the natural biosphere is represented; however, climatological values for LAI also do not fully account for managed land. Nevertheless, the impact of crops is likely to modify the vegetation representation and emission results to a certain degree. The simulation results presented are from a 10-year temporal average with a 500-year offline spin-up phase at a horizontal resolution of T63 (approximately  $1.9^\circ \times 1.9^\circ$  at the Equator). The simulations are climatological, meaning that the same boundary conditions are used for each year of the simulation.

The spatial distribution of the LAI from LPJ-GUESS – shown in Fig. 5 – indicates an elevated LAI of more than  $6 \text{ m}^2 \text{ m}^{-2}$  in the tropical rainforests of the Amazon, Congo and Southeast Asia. The LPJ-GUESS output is also compared with (1) the LAI prescribed for ONEMIS, (2) the LAI prescribed for MEGAN and (3) an external climatology dataset of the global monthly mean LAI averaged over the period from August 1981 to August 2015 (Mao and Yan, 2019). This product uses remotely sensed satellite data from the Moderate Resolution Imaging Spectroradiometer (MODIS) and the Advanced Very High Resolution Radiometer (AVHRR) instruments. Note that each emission scheme utilises its own climatological LAI, and an exchange

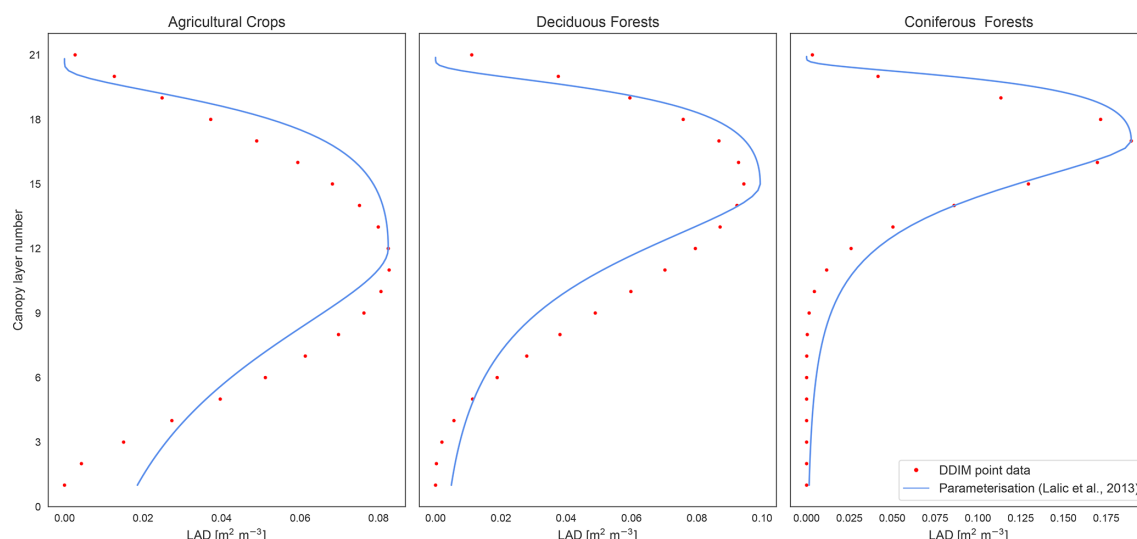


**Figure 4.** LAD distribution for a 21-layer canopy using DDIM point data versus the continuous distribution from the employed parameterisation for the three vegetation classes.

of this dataset results in substantially modified emission fluxes. The difference plots indicate that the climatological LAI used in ONEMIS is generally higher across the globe, while the LAI climatology used in MEGAN is generally lower, especially over the tropics. The external climatological dataset prescribes lower LAI compared to the LAI from LPJ-GUESS. Panel (e) in Fig. 5 shows the global monthly mean LAI from all datasets. LPJ-GUESS exhibits a difference of  $0.73 \text{ m}^2 \text{ m}^{-2}$  between the lowest and highest month, while the variability is  $1.40 \text{ m}^2 \text{ m}^{-2}$  for the ONEMIS dataset,  $0.68 \text{ m}^2 \text{ m}^{-2}$  for the MEGAN dataset and  $0.53 \text{ m}^2 \text{ m}^{-2}$  for the external LAI dataset. This means that the LAI variability from LPJ-GUESS is comparable to the LAI climatology used in MEGAN and the external LAI dataset; however, it differs significantly from the variability in the climatological LAI used in ONEMIS. The foliar density is not presented here, but, by definition, it is a function of the LAI (Eq. 1) and hence shows a similar spatial and temporal distribution. Even though LPJ-GUESS provides potential natural vegetation rather than all present vegetation, a good agreement with climatological LAI is found, particularly the LAI climatology used in MEGAN. Consequently, it is concluded that the current LPJ-GUESS vegetation representation is adequate for estimating BVOC fluxes in ONEMIS and MEGAN but that incorporating land use into the LPJ-GUESS-EMAC configuration will improve current (and future) representations of vegetation and the resulting BVOC estimates.

Figure 6 displays the LAD distribution derived from LPJ-GUESS and the climatology. The climatological LAD (derived from the DDIM model) has been used in the original set-up in ONEMIS to calculate BVOC emission estimates, whereas the LAD from LPJ-GUESS is derived from the parameterisation discussed in Sect. 2.3.3. In LPJ-GUESS, a to-

tal canopy height of 25 m was assumed, and thus, the four LAD layers are classified as follows: bottom canopy layer (LAD 4) represents the LAD between 0–6.25 m, LAD 3 is from 6.25 to 12.50 m, LAD 2 is from 12.50 to 18.75 m, and the top canopy layer (LAD 1) is from 18.75 to 25 m. The values of the four LAD layers (i.e. total canopy) add up to one. The four panels on the right of Fig. 6 show the geographic distribution of LAD from climatology (DDIM model). Even though the LAD canopy distribution from climatology data is oversimplified, it indicates higher densities in the leaf area in the uppermost layers of the canopy over the forested regions found in the tropics and boreal forests in the Northern Hemisphere. The panels on the left show the LAD geographic distribution from LPJ-GUESS at T63. With this approach, a better-resolved geographic distribution for the LAD at the different canopy layers is simulated. Increased LAD in the bottom layer (i.e. all vegetation below 6.25 m) highlights grasslands and desert areas. The layers above show how the LAD changes in the upper sections of the canopy, with plant biomass higher than 20 m mostly found in tropical forest areas. While the climatological LAD remains constant, the LAD from LPJ-GUESS changes from month to month. On average, climatological LAD 1 = 0.21, LAD 2 = 0.32, LAD 3 = 0.40, and LAD 4 = 0.08. LAD 1 from LPJ-GUESS stays constant at around 0.02, and LAD 2 varies between 0.12 (January) and 0.18 (July). LAD 3 and LAD 4 vary a bit but remain close to 0.44 and 0.50, respectively, with no apparent seasonal trends.

Figure 7 shows the fractional coverage required as input for MEGAN. The 12 PFTs from LPJ-GUESS are classified into the four vegetation classes, namely broadleaf trees, needleleaf trees, grass and shrub, and are compared to the corresponding climatology vegetation fraction. The climato-

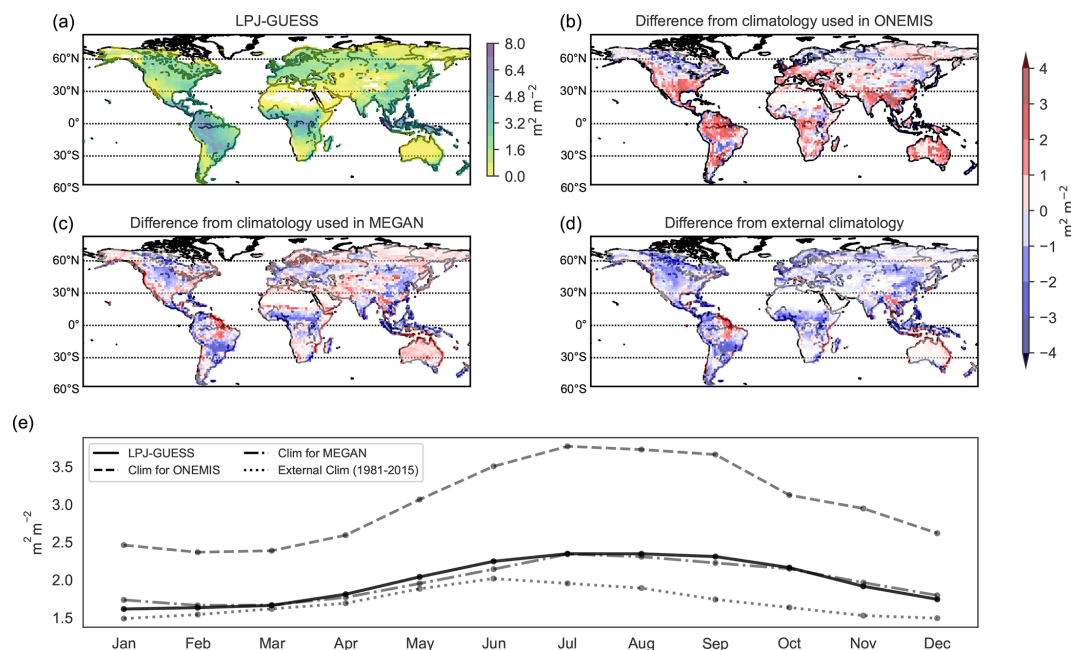


**Figure 5.** Geographic distribution of the LAI from LPJ-GUESS (a) and difference plots (LAI from LPJ-GUESS minus climatological LAI) from climatology used in the standard configuration in ONEMIS and MEGAN (panels b and c). An additional LAI climatology from 1981 to 2015 is also included (d). Panel (e) compares the global monthly averages of all datasets.

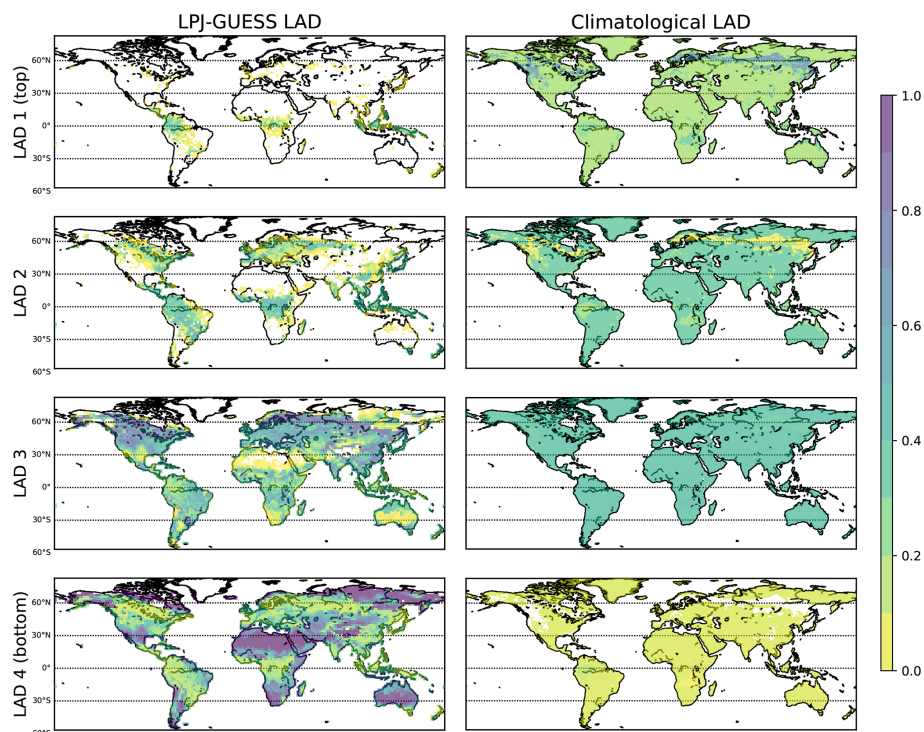


**Figure 6.** LAD fraction at four canopy layers from LPJ-GUESS (left panels) and the DDIM model (right panels). While the climatological LAD is oversimplified and homogeneous, LPJ-GUESS provides a higher-resolved LAD distribution at the four canopy layers.



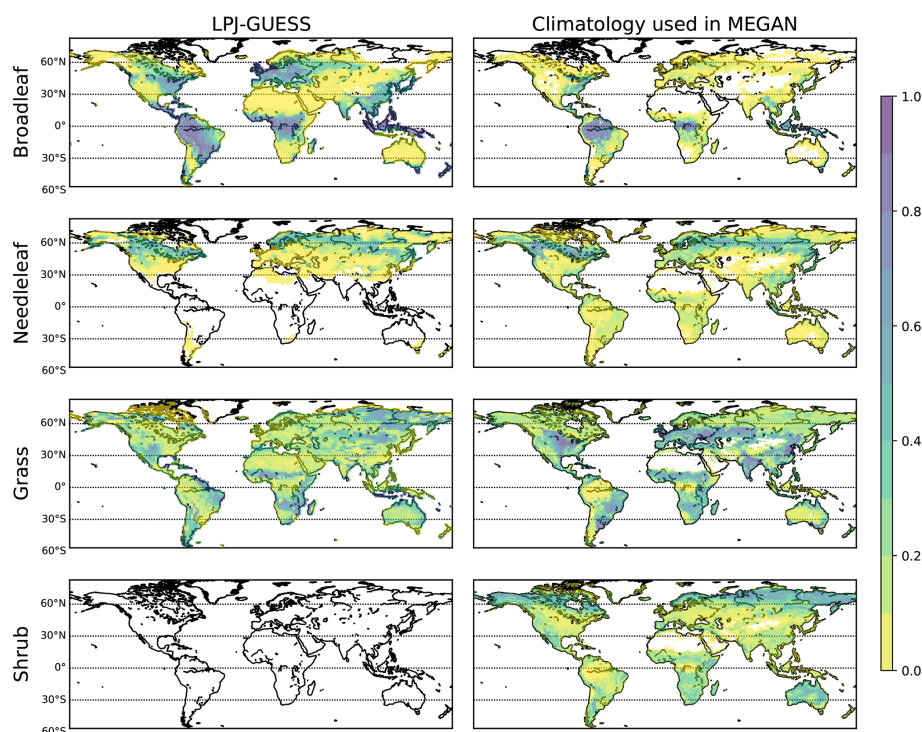


**Figure 7.** Fractional coverage for different vegetation classes used as inputs in MEGAN. The fractional coverage from LPJ-GUESS is displayed in the left panels, while the climatological fractional coverage is displayed in the right panels. Shrub PFTs are currently missing in the applied LPJ-GUESS global PFT set.

logical fractional coverage remains constant throughout the whole simulation, while the fractional coverage from LPJ-GUESS updates from year to year. The global averages of climatological fractional coverage for broadleaf trees, needleleaf trees, grass and shrubs are 0.13, 0.11, 0.23 and 0.14, respectively. LPJ-GUESS provides fractional coverage of 0.35, 0.11, 0.23 and 0 for broadleaf trees, needleleaf trees, grass and shrubs, respectively. Note that shrubs are not included in the currently applied LPJ-GUESS global PFT set; consequently, they are not considered in the applied simulation set-up. Studies by Forrest et al. (2015) did not use explicit shrub PFTs as well, and they have been explicitly included only in more recent studies (e.g. Allen et al., 2020). Even though this leads to less competition among some PFTs in certain regions, this is a limitation of the current study. However, including the new shrub PFTs is planned for future studies. Also, even though temperate needleleaf trees exist in LPJ-GUESS, they are very uncompetitive and thus not well represented in mixed forests.

### 3.2 Global isoprene and monoterpene emissions

#### 3.2.1 Isoprene emissions

Figure 8 presents global isoprene emissions from ONEMIS and MEGAN with dynamic vegetation states from LPJ-GUESS, and offline climatological vegetation inputs, at spa-

tial resolution T63. The simulations have been conducted with fixed prescribed  $\text{CO}_2$  of 348 ppmv (in both the radiation and vegetation schemes). Apart from the exchange of the vegetation, input parameters for the BVOC modules, the simulation set-up, model code and parameter settings are identical in all simulations. All calculations are climatological, i.e. with identical boundary conditions for all years, and the results presented here are from 10 ensemble years.

Panels a and b in Fig. 8 show the geographic distribution of isoprene emission rates (in  $\text{mg m}^{-2} \text{d}^{-1}$ ) using LPJ-GUESS vegetation inputs. Strong isoprene emission fluxes can be seen over South America, central Africa, Southeast Asia and northern Australia, mostly corresponding to high vegetation densities in tropical rainforests. MEGAN emissions are significantly higher, with up to  $90 \text{ mg m}^{-2} \text{d}^{-1}$  over the Amazon rainforest. Such differences in emissions between ONEMIS and MEGAN result from different canopy processes employed by the BVOC modules (see Sect. 2.1). Emission values shown in Fig. 8a and b are from the same simulation, meaning that input parameters (temperature, LAI, etc.) in ONEMIS and MEGAN are identical. Figure 8c and d compare our new emissions using LPJ-GUESS vegetation with emissions using climatological inputs. For both ONEMIS and MEGAN, emissions with dynamic vegetation are lower over tropical areas but higher over Australia compared to emissions using climatology. With climatological vegeta-

tion inputs, ONEMIS exhibits low but significant emissions over deserted regions, particularly the Sahara desert in North Africa, resulting from the poor representation of the LAD distribution in the original model set-up. This is not the case when using dynamic vegetation inputs.

Figure 8e and f depict the temporal profile of global monthly emission totals. In order to capture the true seasonal cycle, values in the Southern Hemisphere were shifted by 6 months before adding fluxes from both hemispheres. Figure 8g and h show the interannual variability in isoprene annual global totals. Over the 10 ensemble years, isoprene emissions appear to peak in the boreal summer months and decrease substantially in the boreal winter months. MEGAN includes a leaf age factor, which accounts for reduced emissions for young and old leaves based on observed LAI change. This explains the slight decrease in MEGAN emissions from April to May to June.

Over the 10-year simulation period considered, the global annual total isoprene fluxes from ONEMIS were found to be  $546 \text{ Tg yr}^{-1}$  (standard deviation (SD) =  $8 \text{ Tg yr}^{-1}$ ) with dynamic vegetation and  $558 \text{ Tg yr}^{-1}$  (SD =  $7 \text{ Tg yr}^{-1}$ ) with climatological inputs. MEGAN estimated  $657 \text{ Tg yr}^{-1}$  (SD =  $11 \text{ Tg yr}^{-1}$ ) with dynamic vegetation and  $631 \text{ Tg yr}^{-1}$  (SD =  $11 \text{ Tg yr}^{-1}$ ) with climatological vegetation inputs. The higher standard deviation when using LPJ-GUESS inputs indicates higher interannual variability in isoprene fluxes. While the year-to-year variability with climatological inputs is only determined by surface temperature and shortwave radiation (see Fig. 2), the interannual variability with LPJ-GUESS inputs is also influenced by interannual changes in vegetation states estimated in LPJ-GUESS. Jöckel et al. (2016) reported isoprene annual emissions of  $488\text{--}624 \text{ Tg}$  using ONEMIS, while other studies estimated fluxes of  $642 \text{ Tg yr}^{-1}$  (Shim et al., 2005) using 73 prescribed vegetation types,  $571 \text{ Tg yr}^{-1}$  (Guenther et al., 2006) using inventories and Olson ecoregion land covers,  $467 \text{ Tg yr}^{-1}$  (Arneth et al., 2007a) using 10 PFTs from LPJ-GUESS and, more recently,  $594 \text{ Tg yr}^{-1}$  using 16 PFTs (Sindelarova et al., 2014). It is important to note that no scaling factors were applied in our simulations, even though global annual totals from models are often scaled in atmospheric chemistry studies. For example, Pozzer et al. (2022) estimated  $464 \text{ Tg}$  of isoprene in the year 2010 using a MEGAN-EMAC set-up but employed a global scaling factor of 0.6. This means that the original emissions are similar to our MEGAN fluxes with climatological inputs. In general, our LPJ-GUESS-driven BVOC emissions in EMAC agree with past modelling estimates with similar spatial and temporal patterns.

### 3.2.2 Monoterpene emissions

Results for monoterpene emissions are shown in Fig. 9. Panels a and b present the spatial distribution of monoterpene emission rates (in  $\text{mg m}^{-2} \text{ d}^{-1}$ ) from ONEMIS and MEGAN, while Fig. 9c and d show the difference in the

emission fluxes using climatological vegetation inputs. Elevated emission rates are also found over tropical rainforest regions, with ONEMIS prescribing much higher emission rates compared to MEGAN. The difference plots indicate that monoterpene emissions from ONEMIS are significantly higher with climatological inputs, except for some areas over southern Brazil and central Africa. Similarly, MEGAN generally prescribes higher emissions with climatological vegetation inputs compared to LPJ-GUESS inputs. ONEMIS emissions over deserted regions in north Africa and central Australia appear to be better resolved with dynamic vegetation, since ONEMIS with climatology inputs still attributes significant emission rates over such regions where vegetation is absent.

Monoterpene emission fluxes in ONEMIS only depend on the foliar density profile (i.e.  $\text{DM} \times \text{LAD}$ ) and surface temperature. The high dependence of monoterpene emissions on foliar density explains both the lower seasonal variability and the lower yearly fluxes compared to emissions with climatological vegetation inputs. The lower magnitudes in monoterpene fluxes from MEGAN with dynamic vegetation result from the lack of representation of shrubs and needle-leaf tree PFTs in LPJ-GUESS, where such species are known to be strong emitters of monoterpenes. The seasonal variation, however, is satisfying, and the fact that the fractional coverages computed in LPJ-GUESS are dynamic (updating on a yearly time step) makes this set-up suitable for studying long-term variations in emissions. Annual totals from ONEMIS were found to be  $102 \text{ Tg yr}^{-1}$  (SD =  $1 \text{ Tg yr}^{-1}$ ) with dynamic vegetation inputs and  $175 \text{ Tg yr}^{-1}$  (SD =  $2 \text{ Tg yr}^{-1}$ ) with climatological inputs. MEGAN prescribes  $54 \text{ Tg yr}^{-1}$  (SD =  $0.7 \text{ Tg yr}^{-1}$ ) and  $76 \text{ Tg yr}^{-1}$  (SD =  $0.9 \text{ Tg yr}^{-1}$ ) with dynamic and climatological inputs, respectively. Guenther et al. (2012) gives a global annual monoterpene emission of  $157 \text{ Tg}$ , while Sindelarova et al. (2014) reported annual total emissions of monoterpenes ranging between 89 and  $102 \text{ Tg yr}^{-1}$  over a 30-year simulation period. Arneth et al. (2007a) reported  $36 \text{ Tg yr}^{-1}$ .

### 3.2.3 BVOC emissions from LPJ-GUESS

This section presents isoprene and monoterpene emission fluxes from the semi-processed-based module in LPJ-GUESS for comparison with the empirically based emissions from ONEMIS and MEGAN in the coupled model system. The LPJ-GUESS routine runs entirely within the LPJ-GUESS framework, meaning that emission values are provided on a daily basis. In this study, the LPJ-GUESS BVOC routine uses DTR computed in EMAC instead of climatological DTR (see Sect. 2.3). Panels a and b in Fig. 10 show the spatial distribution of isoprene and monoterpene emission rates from the LPJ-GUESS BVOC emissions routine. Figure 10c and d show the monthly total emissions from LPJ-GUESS and emissions from ONEMIS and MEGAN for comparison.



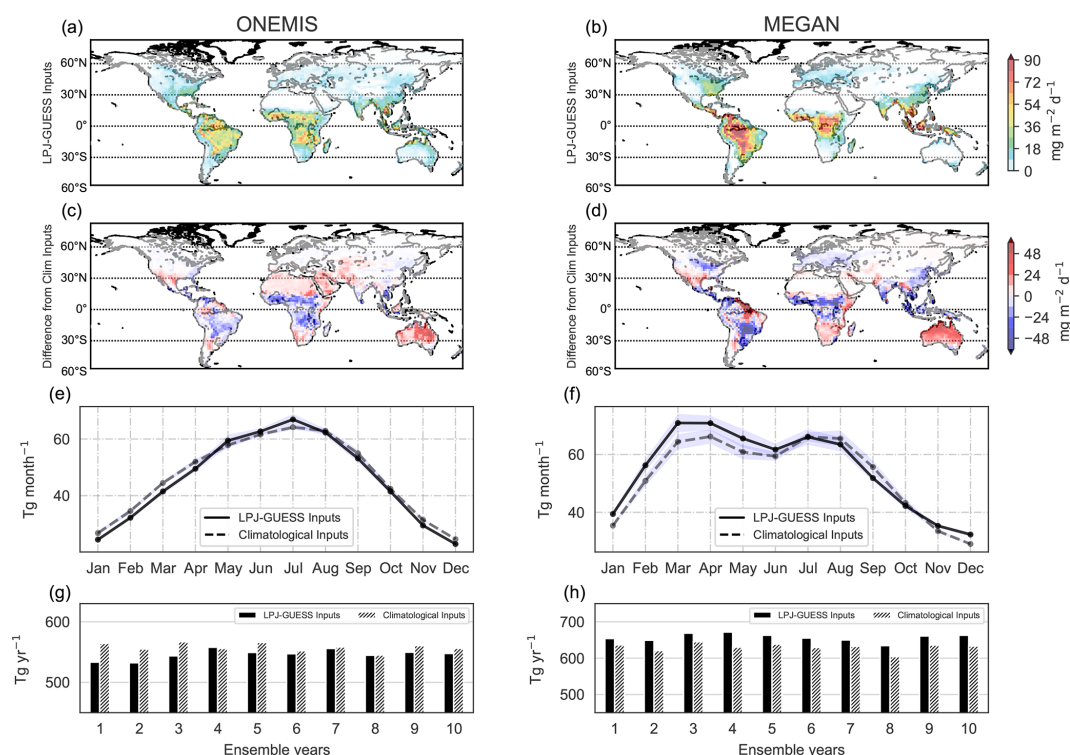


**Figure 8.** Spatial distribution of monthly isoprene emissions ( $\text{mg m}^{-2} \text{d}^{-1}$ ) averaged over 10 ensemble years with LPJ-GUESS vegetation inputs from ONEMIS and MEGAN (panels a and b). Panels (c) and (d) show the difference in the emission flux compared to emissions from ONEMIS and GUESS with climatological vegetation inputs. The temporal profile of isoprene global totals in teragrams per month are depicted in panels (e) and (f), and global annual totals ( $\text{Tg yr}^{-1}$ ) for 10 ensemble years are shown in panels (g) and (h).

Monthly isoprene emissions from LPJ-GUESS range from 48.3 Tg in December to 88.2 Tg in July, whereas monthly monoterpene emissions range from 1.8 Tg in January to 7.3 Tg in July. Figure 10e and f show yearly isoprene and monoterpene totals from LPJ-GUESS, ONEMIS and MEGAN for 10 ensemble years. The mean isoprene annual emission flux is  $750 \text{ Tg yr}^{-1}$  ( $\text{SD} = 17 \text{ Tg yr}^{-1}$ ), while for monoterpenes it is  $50 \text{ Tg yr}^{-1}$  ( $\text{SD} = 1 \text{ Tg yr}^{-1}$ ). The process-based isoprene emissions from LPJ-GUESS are marginally higher compared to the empirically based emissions from ONEMIS and MEGAN. For monoterpenes, emissions from LPJ-GUESS are similar to MEGAN emissions, while ONEMIS emissions are twice as much.

Currently, both empirical (e.g. Guenther et al., 2006) and process-based models (e.g. Niinemets et al., 1999; Bäck et al., 2005; Arneth et al., 2007b; Schurgers et al., 2009) are widely used to model and assess global BVOC emission estimates. Process-based models consider the emission inhibition from carbon and energy availability, allowing for some stress effects to be taken into consideration. In general, empirically based models suggest increased BVOC emissions in future climate scenarios resulting from temperature sensitivity and enhanced vegetation activity in a  $\text{CO}_2$ -rich atmosphere (Sanderson et al., 2003; Naik et al., 2004; Lathiere et al., 2005). In contrast, process-based models indicate

that  $\text{CO}_2$  inhibition of the leaf–isoprene metabolism can be large enough to offset increases in emissions (Arneth et al., 2007b; Heald et al., 2009). More recent laboratory studies provide evidence that certain plant species emit more isoprene in high  $\text{CO}_2$  environments (e.g. Sun et al., 2013), indicating that there are still some gaps in the understanding of biochemical regulation of BVOC leaf emissions incorporated in such models. Grote and Niinemets (2007) compares the two model categories and argues that, in non-stressful conditions, empirical and process-based emission models predict BVOC emission dependencies on light and temperature in a similar way. A modelling study also showed that, regardless of whether  $\text{CO}_2$  inhibitory effects are considered or not, temperature is the most important driver for increased isoprene emissions (Cao et al., 2021). In this study, it is shown that, even though process-based emissions from LPJ-GUESS might differ (in magnitude) from empirically based emissions in EMAC, the monthly distributions in emissions are similar (Fig. 10c and d). Even though emissions from ONEMIS and MEGAN in EMAC are empirically based, emissions in the new coupled configuration are now sensitive to vegetation changes, which is a substantial improvement over emissions with prescribed vegetation information in the previous model configuration.

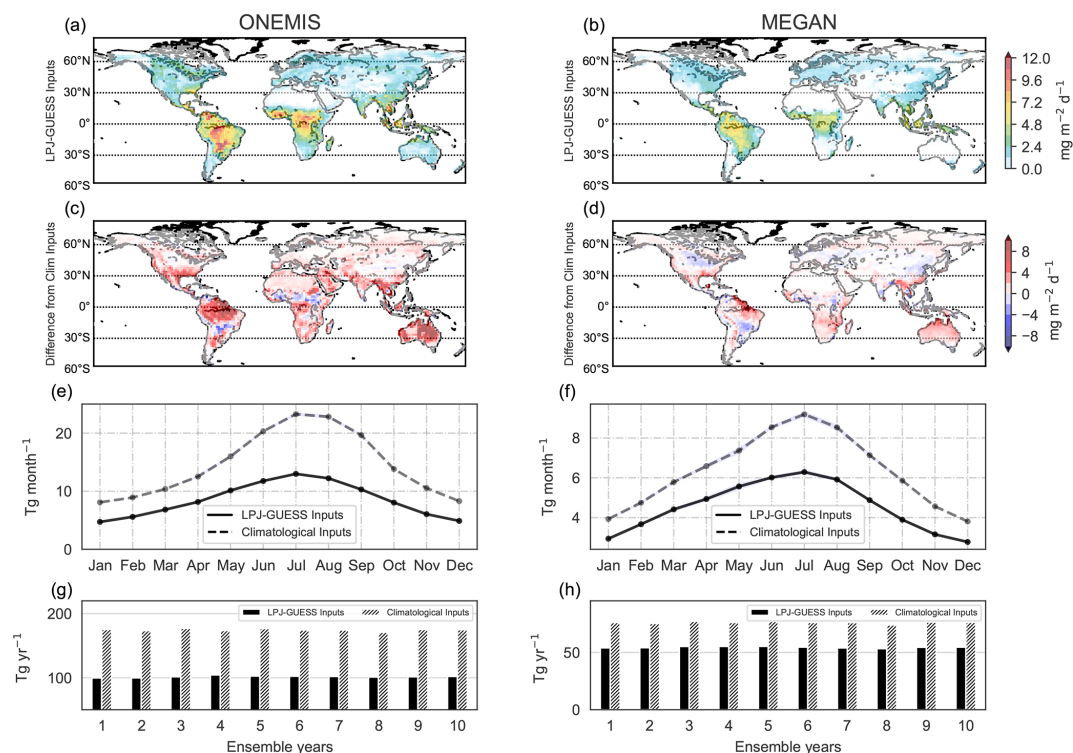


**Figure 9.** Same as Fig. 8 but for monoterpenes.

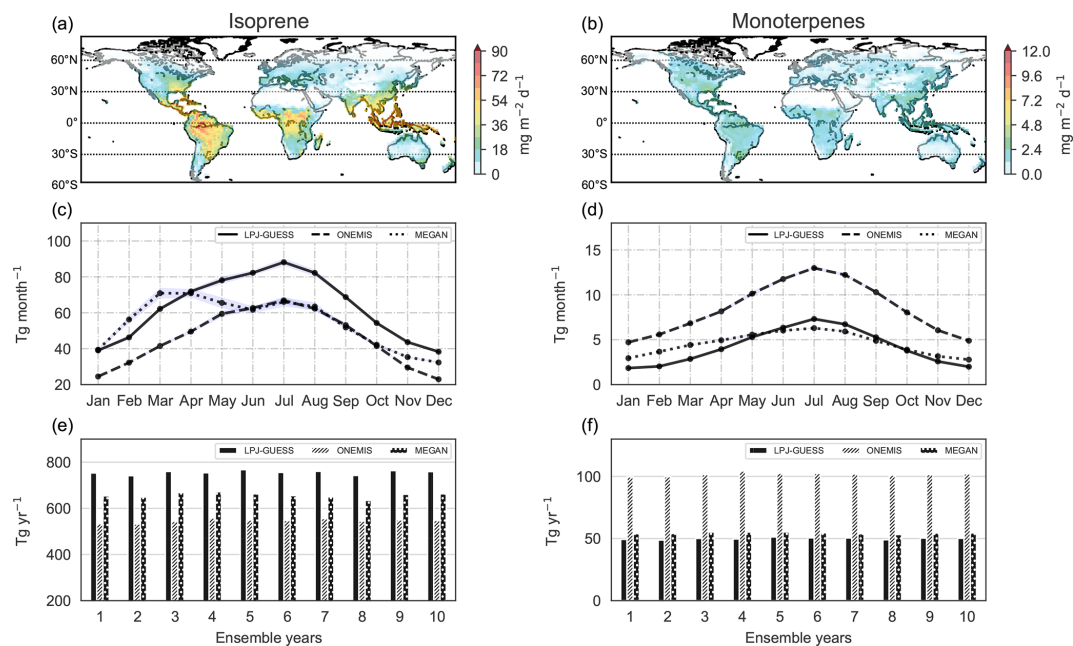


**Figure 10.** Spatial distribution of isoprene and monoterpene emissions from LPJ-GUESS at a spatial resolution of T63 (panels a and b). Isoprene and monoterpene mean monthly totals in teragrams per month from LPJ-GUESS, ONEMIS and MEGAN (panels c and d) and annual totals in teragrams per year for 10 ensemble years (panels e and f).

**Table 1.** Prescribed CO<sub>2</sub> in the radiation and vegetation schemes for different studies.

Study	CO <sub>2</sub> in radiation scheme	CO <sub>2</sub> in vegetation scheme
Ref	348 ppmv	348 ppmv
Bio × 2	348 ppmv	696 ppmv
Atm × 2	696 ppmv	348 ppmv
Both × 2	696 ppmv	696 ppmv

### 3.3 Emission sensitivity to double CO<sub>2</sub> scenarios

In this section, the variability in global isoprene and monoterpene emission estimates in doubling CO<sub>2</sub> scenarios is investigated. In particular, the CO<sub>2</sub> fertilisation and temperature effects are evaluated by prescribing different CO<sub>2</sub> values in the radiation and vegetation schemes in the coupled model set-up, as described in Sect. 2.4. The scope here is not to develop realistic future scenarios but rather to assess the model's sensitivity to atmospheric and vegetation CO<sub>2</sub> – hence the use of doubling scenarios. Four experiments were conducted to explore the impact of doubling CO<sub>2</sub> scenarios (both in the radiation and vegetation scheme) on isoprene and monoterpene emission rates. Ref is the reference simulation, with 348 ppmv [CO<sub>2</sub>] in both schemes. Table 1 lists the CO<sub>2</sub> levels prescribed for each study. The analyses shown here are based on 10 years of data from 50-year simulations with constant boundary conditions and a 500-year offline spin-up phase.

#### 3.3.1 Surface temperature in 2 × CO<sub>2</sub> in the radiation scheme

The temperature sensitivity of BVOC emissions is studied by doubling the prescribed CO<sub>2</sub> value in the radiation scheme. This results in a consistent global increase in the surface temperature of up to 4 °C in conjunction with the prescribed enhanced SST and sea ice coverage (see Appendix A).

#### 3.3.2 Vegetation response to 2 × CO<sub>2</sub> scenarios

The LAI can be used as a marker for vegetation activity. Figure 11 displays LAI estimates from LPJ-GUESS for the reference study, Ref, and also shows how LAI values in the other studies compare to it. Bio × 2 indicates consistently increased vegetation activity when doubling the prescribed CO<sub>2</sub> in the vegetation scheme. This is the CO<sub>2</sub> fertilisation effect. The LAI in Atm × 2 decreases as a result of warmer temperatures and higher losses of soil moisture (reported elsewhere; e.g. Dermody et al., 2007; Sun et al., 2015). In Both × 2, with 696 ppmv [CO<sub>2</sub>] in both the vegetation and radiation scheme, an overall rise in LAI compared to the Ref simulation is found, except for some regions in North America, western Brazil and southern Europe. In these areas, the water stress from higher surface temperatures results in an

overall decline in the vegetation, e.g. grass species take over forested areas, partly decreasing the LAI in the region. To this end, this model set-up can be used to analyse changes in BVOC emissions due to shifts in vegetation patterns in future climate scenarios.

#### 3.3.3 Global BVOC emissions

Figure 12 shows the geographic distribution of isoprene emission rates (in mg m<sup>-2</sup> d<sup>-1</sup>) averaged over 10 ensemble years for Ref and difference plots for Bio × 2, Atm × 2, and Both × 2 using climatological and dynamic vegetation inputs using ONEMIS and MEGAN. The bottom panels (Fig. 12q, r, s, and t) show the averaged emission rates for distinct latitude bands (0–30° S, 0–30° N, 30–60° N) for all studies during the same period, from left to right. It is found that in Bio × 2, isoprene emissions increased only when using dynamic vegetation inputs in both ONEMIS and MEGAN (Fig. 12b and j) are applied. In contrast to the prescribed climatological vegetation data, the LPJ-GUESS coupled set-up is sensitive to increased CO<sub>2</sub>, which subsequently leads to higher emissions. Note that, in this scenario, ONEMIS attributes lower emission values over the tropics (Fig. 12b). Isoprene emissions are more dependent on light than on leaf area, so increased foliage may limit isoprene emissions in closed canopies such as in dense tropical rain forests (Guenther et al., 2006). This is not the case for open canopies, where increased foliage drastically enhances isoprene emissions. This effect is not well captured by MEGAN (Fig. 12j), given that here the PCEE algorithm is employed whereas the canopy environment model only considers above-canopy radiation and is not sensitive to sun and shaded leaves at each canopy depth. In Atm × 2, temperature effects on isoprene emissions are found, while in Both × 2 we see how the combined effects of CO<sub>2</sub> fertilisation and temperature become obvious. The bar plots reveal that, in places where most of the global emissions occur, i.e. between 0 and 30° S, the emission was the highest in Both × 2, with an average emission rate of 27.3 mg m<sup>-2</sup> d<sup>-1</sup> (ONEMIS) and 44.3 mg m<sup>-2</sup> d<sup>-1</sup> (MEGAN). Given the empirical nature of ONEMIS and MEGAN, both set-ups give a consistent increase in isoprene fluxes in elevated temperatures (Atm × 2). However, with LPJ-GUESS inputs, differences in the emission fluxes are found that also result from vegetation dynamics, e.g. a decrease in fluxes from lower vegetation activity caused by water stresses. This highlights the advantage of having BVOC fluxes derived from dynamic vegetation states rather than prescribed boundary conditions.

In Fig. 13, similar behaviour in the monoterpene emission estimates is depicted for all studies. Monoterpene emission rates increase in Bio × 2 only for scenarios with dynamic vegetation due to CO<sub>2</sub> fertilisation. A worldwide increase in monoterpene fluxes in Atm × 2 is detected with higher surface temperatures using climatological inputs. However, with dynamic vegetation inputs, a less substantial rise, and a drop

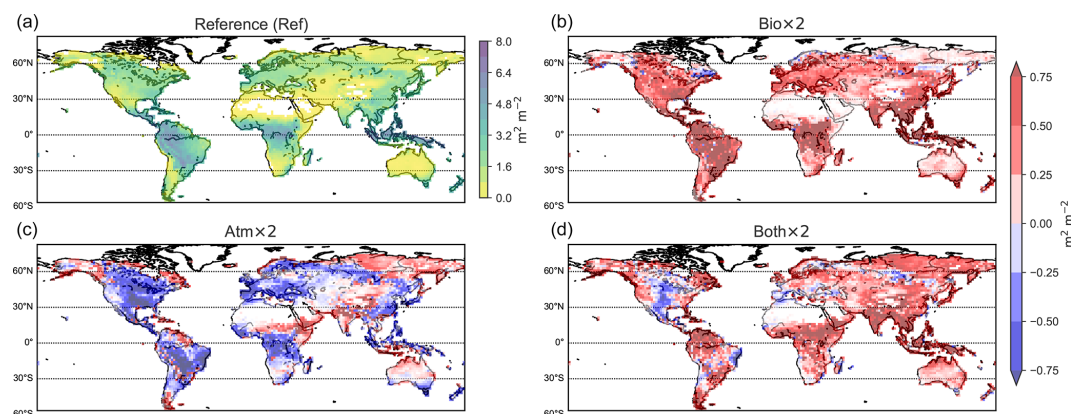


**Figure 11.** Geographic distribution of the LAI for the reference study (Ref) and difference plots.  $\text{Bio} \times 2 - \text{Ref}$  (b),  $\text{Atm} \times 2 - \text{Ref}$  (c) and  $\text{Both} \times 2 - \text{Ref}$  (d) are shown.

in fluxes in certain regions, is determined. In  $\text{Both} \times 2$ , an increase in monoterpene emission rates is found as a result of the combined influence of temperature and  $\text{CO}_2$  fertilisation.

#### 4 Conclusions

The development of ESMs allows for a far more detailed analysis of a fully coupled and dynamic system addressing many complex biosphere–atmosphere interactions governed by BVOC emissions and thus shedding more light on the significance of such processes on global climate change and air quality. In this work, further development has been made towards producing a new atmospheric-chemistry-enabled ESM by coupling an atmospheric-chemistry-enabled atmosphere–ocean general circulation model (AOGCM) with a DGVM. This work also explores, for the first time, partial bi-directional interactions between the two modelling systems via BVOC emissions, building on recent technical developments (Forrest et al., 2020) that enabled one-way coupled simulations (in which climate information generated by EMAC is used to force LPJ-GUESS, but no land surface information is relayed back to EMAC). The updated model version described in this work allows computations of isoprene and monoterpene emissions based on dynamic vegetation states running on the EMAC time step. This is a substantial improvement compared to the earlier set-up in which BVOC emissions were only based on offline vegetation information and not coupled with dynamic vegetation states. The BVOC module in LPJ-GUESS (used in this study only to compare our new emissions in EMAC; Fig. 10) uses dynamic vegetation information but only provides daily average emissions, and these emissions are not yet integrated into EMAC.

Results show that the LAI and subsequent foliar density estimations from LPJ-GUESS are comparable to climatological datasets used as boundary layer conditions in the MEGAN-EMAC standalone configuration and an external

LAI climatology from 1981 to 2015. The LAI employed in the original ONEMIS-EMAC set-up, on the other hand, differs significantly in terms of magnitude and monthly variability. Such differences in the LAI inputs led to lower isoprene and monoterpene emissions using the coupled model set-up compared to the standalone configuration. The representation of the LAD distribution from the new parameterisation employed in LPJ-GUESS also gives a more realistic LAD profile compared to the oversimplified datasets used by the standard ONEMIS set-up. Given that our coupling only involves vegetative information going into ONEMIS and MEGAN in EMAC, our climate biases are considered to be consistent with those discussed in Forrest et al. (2020).

The new MEGAN-LPJ-GUESS configuration yielded satisfactory isoprene fluxes as well, with a monthly distribution comparable to MEGAN emissions with climatological inputs. Monoterpene emissions from the MEGAN-LPJ-GUESS set-up also give meaningful monthly variability with lower magnitudes compared to emissions with climatological inputs, given that the new set-up lacks emission contributions from shrubs and needleleaf tree PFTs in mixed forests. Future studies may include region-specific PFT groups (including shrub PFTs); however, for this study, the global PFT set is kept unchanged. Global isoprene emission estimates from the coupled model configuration, using both ONEMIS and MEGAN, give realistic global variability, corresponding to emissions with prescribed vegetation boundary conditions. The emission magnitudes are also comparable to modelled fluxes found in the literature and can be adjusted accordingly with global scaling factors for specific atmospheric chemistry studies. The new vegetation-sensitive emissions from ONEMIS and MEGAN agree with previous approaches with respect to the spatial and temporal patterns but provide more consistency and higher temporal resolution as required for interactive atmospheric chemistry simulations.

This study finds that (1) differences in BVOC emissions with implemented dynamic vegetation result almost entirely



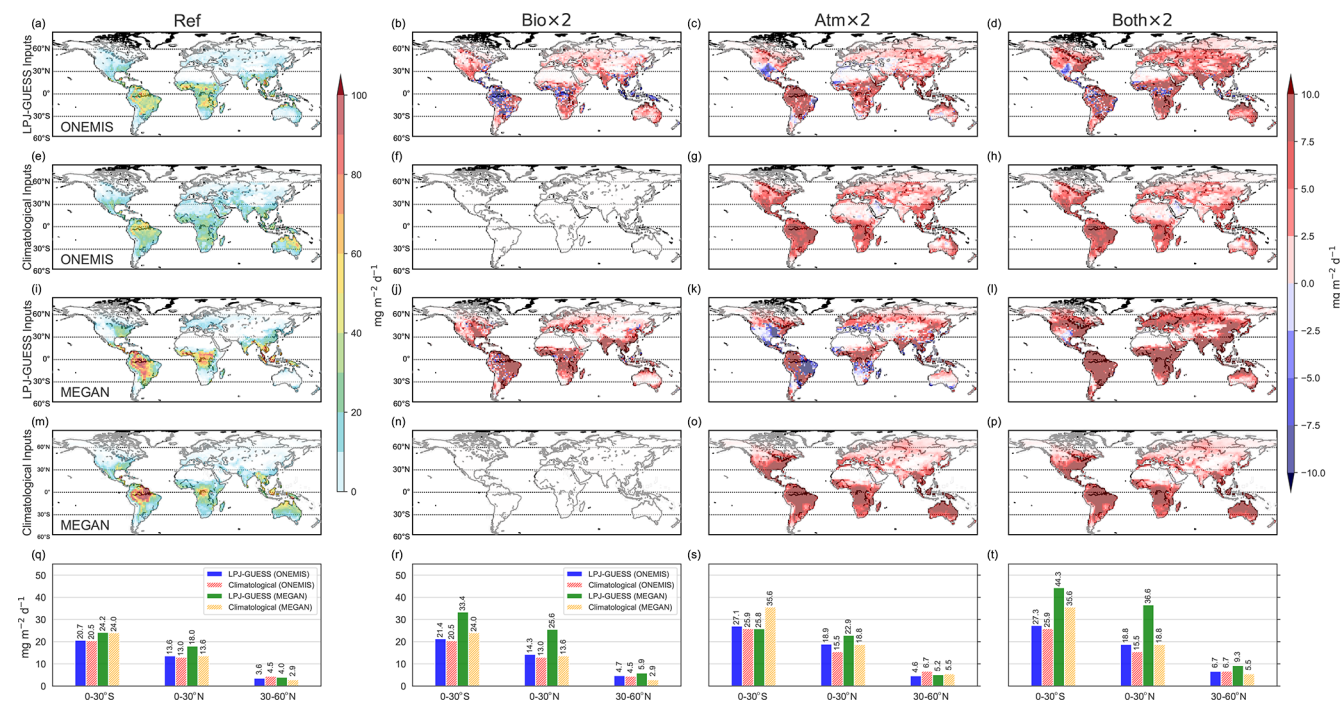


**Figure 12.** Global isoprene emission estimates from ONEMIS and MEGAN with LPJ-GUESS vegetation inputs and climatological inputs for the reference study (Ref) (a, e, i, m) and difference plots for  $\text{Bio} \times 2$  (b, f, j, n),  $\text{Atm} \times 2$  (c, g, k, o) and  $\text{Both} \times 2$  (d, h, l, p). The panels at the bottom (q, r, s, t) display the emission flux averages (in  $\text{mg m}^{-2} \text{d}^{-1}$ ) over the latitude bands  $0-30^\circ \text{S}$ ,  $0-30^\circ \text{N}$ ,  $30-60^\circ \text{N}$ .

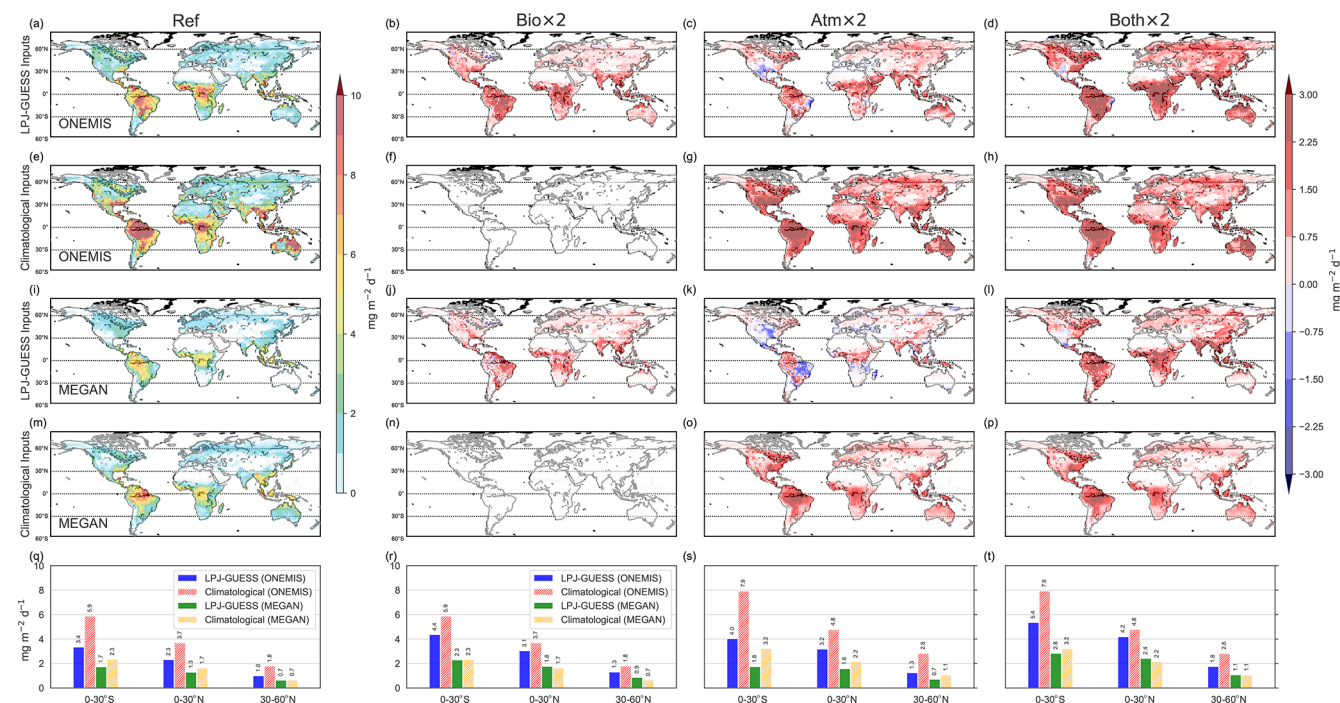


**Figure 13.** Same as Fig. 12 but for monoterpenes.

from changes in the input LAI, and the (2) dynamic vegetation increase the interannual variability in BVOC emissions by introducing new variability from dynamic vegetation states. These findings are comparable to those of Levis et al. (2003), where dynamic vegetation was implemented in the Community Climate System Model (CCSM).

CO<sub>2</sub> sensitivity studies also suggest that both isoprene and monoterpene emissions rise with warmer climatic scenarios ( $2 \times \text{CO}_2$  in the radiation scheme); however, only the coupled configuration showed reduced emissions in some locations. The lower emissions result from the vegetation response to water stresses in a warmer climate. The new coupled model also allows for sensitivity studies for CO<sub>2</sub> fertilisation effects and indicates an increase in both isoprene and monoterpene emission rates in  $2 \times \text{CO}_2$  scenarios in the vegetation scheme due to enhanced vegetation activity in a CO<sub>2</sub>-rich atmosphere. This work provides evidence that the improved ESM, featuring dynamic vegetation, gives realistic BVOC emission estimates on a global scale, based on dynamic vegetation states, enabling further research into atmosphere–biosphere interactions and feedbacks with this model configuration.

## Appendix A: Surface temperature at doubling CO<sub>2</sub> scenarios

Figure A1 illustrates temperatures (°C) at the lowermost vertical level in EMAC at spatial resolution T63 with prescribed CO<sub>2</sub> of 348 ppmv in the top panel and 696 ppmv in the middle panel. A plot comparing the reference simulations to the  $2 \times \text{CO}_2$  simulations is given in the lower panel of Fig. A1.

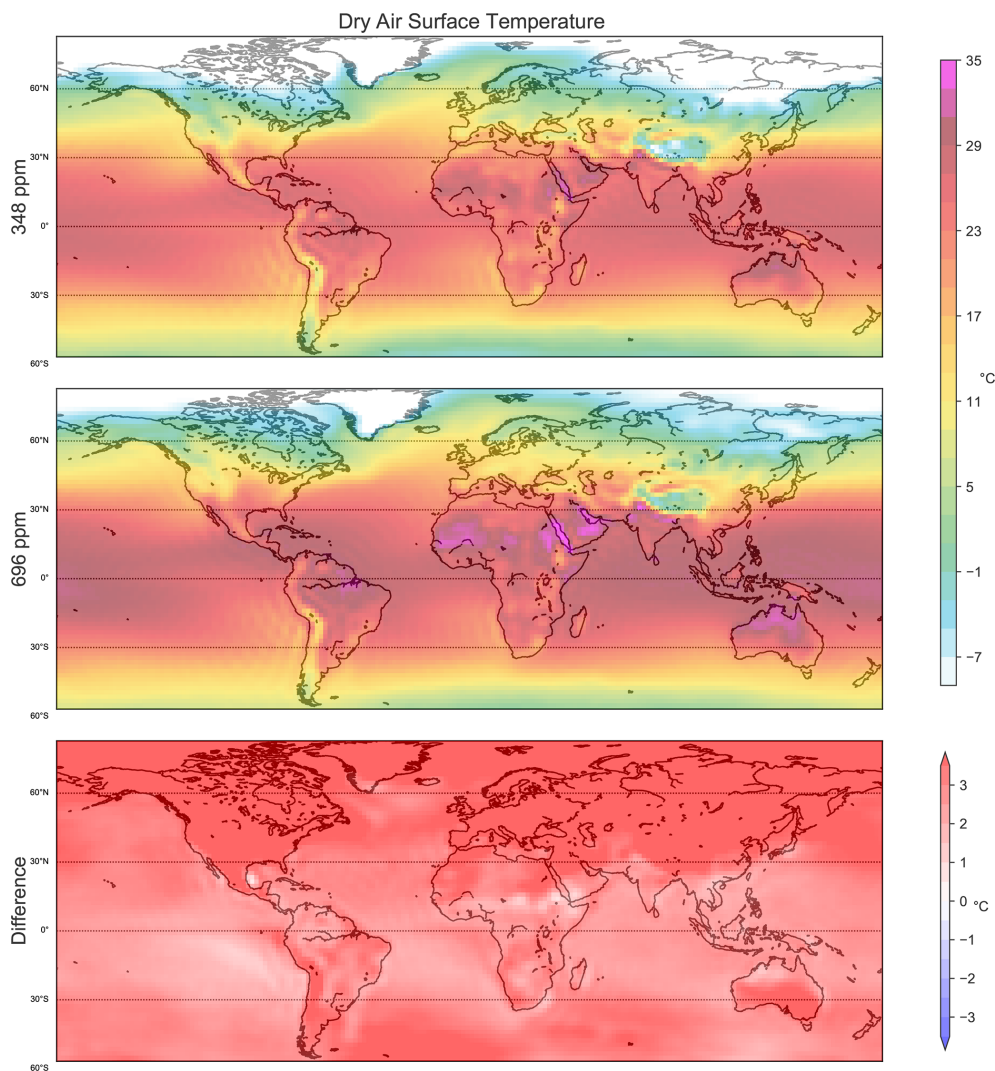


**Figure A1.** Surface temperature (°C) at spatial resolutions T63. In the radiation scheme, the first model configuration utilises a CO<sub>2</sub> volume mixing ratio of 348 ppm (parts per million), whereas the second set-up uses 696 ppm.



**Code availability.** The Modular Earth Submodel System (MESSy) is continuously developed and applied by a consortium of institutions. MESSy is licensed to all affiliates of institutions that are members of the MESSy Consortium, as is access to the source code. Institutions can become a member of the MESSy Consortium by signing the MESSy Memorandum of Understanding. More information can be found on the MESSy Consortium website (<http://www.messy-interface.org>, last access: 14 January 2023). LPJ-GUESS is used and developed globally; however, development is overseen at Lund University's Department of Physical Geography and Ecosystem Science in Sweden. Model codes can be made available to collaborators on entering into a collaboration agreement with the acceptance of certain conditions. Given that both MESSy and LPJ-GUESS are restricted, the code used here is archived with a restricted-access DOI (<https://doi.org/10.5281/zenodo.6772205>; Vella et al., 2022). The code will not be made publicly available, and sharing will be made possible only by the approval of the authors. The code described in this work has already been incorporated into the official development branch of the EMAC modelling system and will therefore be part of all future released versions.

**Data availability.** The datasets from this work will be made available on request to the corresponding author.

**Author contributions.** RV and HT performed the model coupling. RV performed the simulations and analysis. MF and JL contributed to the overall model development and interpretation of the results. RV wrote the article, with significant inputs from all co-authors.

**Competing interests.** At least one of the (co-)authors is a member of the editorial board of *Geoscientific Model Development*. The peer-review process was guided by an independent editor, and the authors also have no other competing interests to declare.

**Disclaimer.** Publisher's note: Copernicus Publications remains neutral with regard to jurisdictional claims in published maps and institutional affiliations.

**Acknowledgements.** This research was conducted using the supercomputer MOGON and/or advisory services offered by Johannes Gutenberg University Mainz (<https://hpc.uni-mainz.de/>, last access: 14 January 2023), which is a member of the AHRP (Alliance for High Performance Computing in Rhineland-Palatinate; <https://www.ahrp.info/>, last access: 14 January 2023) and Gauß-Allianz e.V. Ryan Vella thanks Andrea Pozzer (Max Planck Institute for Chemistry, Mainz), for technical support to implement MEGAN in the new model configuration. This work has been supported by the Max Planck Graduate Center with the Johannes-Gutenberg-Universität Mainz (MPGC). We also acknowledge funding from the Carl Zeiss Foundation for Holger Tost. Finally, we thank the three anonymous reviewers and the handling editor for their helpful comments.

**Financial support.** Ryan Vella has been supported by the Johannes-Gutenberg-Universität Mainz (MPGC), and Holger Tost has been supported by the Carl Zeiss Foundation.

The article processing charges for this open-access publication were covered by the Max Planck Society.

**Review statement.** This paper was edited by Jinkyu Hong and reviewed by three anonymous referees.

## References

- Alessandri, A., Catalano, F., De Felice, M., Van Den Hurk, B., Reyes, F. D., Boussetta, S., Balsamo, G., and Miller, P. A.: Multi-scale enhancement of climate prediction over land by increasing the model sensitivity to vegetation variability in EC-Earth, *Clim. Dynam.*, 49, 1215–1237, 2017.
- Allen, J. R., Forrest, M., Hickler, T., Singarayer, J. S., Valdes, P. J., and Huntley, B.: Global vegetation patterns of the past 140,000 years, *J. Biogeogr.*, 47, 2073–2090, 2020.
- Arey, J., Winer, A. M., Atkinson, R., Aschmann, S. M., Long, W. D., Morrison, C. L., and Olszyk, D. M.: Terpenes emitted from agricultural species found in California's Central Valley, *J. Geophys. Res.-Atmos.*, 96, 9329–9336, 1991.
- Arneth, A., Miller, P. A., Scholze, M., Hickler, T., Schurgers, G., Smith, B., and Prentice, I. C.: CO<sub>2</sub> inhibition of global terrestrial isoprene emissions: Potential implications for atmospheric chemistry, *Geophys. Res. Lett.*, 34, L18813, <https://doi.org/10.1029/2007GL030615>, 2007a.
- Arneth, A., Niinemets, Ü., Pressley, S., Bäck, J., Hari, P., Karl, T., Noe, S., Prentice, I. C., Serça, D., Hickler, T., Wolf, A., and Smith, B.: Process-based estimates of terrestrial ecosystem isoprene emissions: incorporating the effects of a direct CO<sub>2</sub>-isoprene interaction, *Atmos. Chem. Phys.*, 7, 31–53, <https://doi.org/10.5194/acp-7-31-2007>, 2007b.
- Atkinson, R.: Atmospheric chemistry of VOCs and NO<sub>x</sub>, *Atmos. Environ.*, 34, 2063–2101, 2000.
- Atkinson, R. and Arey, J.: Gas-phase tropospheric chemistry of biogenic volatile organic compounds: a review, *Atmos. Environ.*, 37, 197–219, 2003.
- Bäck, J., Hari, P., Hakola, H., Juurola, E., and Kulmala, M.: Dynamics of monoterpene emissions in *Pinus sylvestris* during early spring, *Boreal Environ. Res.*, 10, 409–424, 2005.
- Bai, J., Baker, B., Liang, B., Greenberg, J., and Guenther, A.: Isoprene and monoterpene emissions from an Inner Mongolia grassland, *Atmos. Environ.*, 40, 5753–5758, 2006.
- Bonan, G. B.: Forests and climate change: forcings, feedbacks, and the climate benefits of forests, *Science*, 320, 1444–1449, 2008.
- Box, E.: Foliar biomass: data base of the International Biological Program and other sources [Forest types, environmental conditions, Japan], 1981.
- Cao, Y., Yue, X., Liao, H., Yang, Y., Zhu, J., Chen, L., Tian, C., Lei, Y., Zhou, H., and Ma, Y.: Ensemble projection of global isoprene emissions by the end of 21st century using CMIP6 models, *Atmos. Environ.*, 267, 118766, <https://doi.org/10.1016/j.atmosenv.2021.118766>, 2021.

- Cortinovis, J., Solmon, F., Serça, D., Sarrat, C., and Rosset, R.: A simple modeling approach to study the regional impact of a Mediterranean forest isoprene emission on anthropogenic plumes, *Atmos. Chem. Phys.*, 5, 1915–1929, <https://doi.org/10.5194/acp-5-1915-2005>, 2005.
- Dermody, O., Weltzin, J. F., Engel, E. C., Allen, P., and Norby, R. J.: How do elevated  $[\text{CO}_2]$ , warming, and reduced precipitation interact to affect soil moisture and LAI in an old field ecosystem?, *Plant Soil*, 301, 255–266, 2007.
- Dietmüller, S., Jöckel, P., Tost, H., Kunze, M., Gellhorn, C., Brinkop, S., Frömming, C., Ponater, M., Steil, B., Lauer, A., and Hendricks, J.: A new radiation infrastructure for the Modular Earth Submodel System (MESSy, based on version 2.51), *Geosci. Model Dev.*, 9, 2209–2222, <https://doi.org/10.5194/gmd-9-2209-2016>, 2016.
- Evans, R. C., Tingey, D. T., Gumpertz, M. L., and Burns, W. F.: Estimates of isoprene and monoterpene emission rates in plants, *Bot. Gaz.*, 143, 304–310, 1982.
- Flato, G., Marotzke, J., Abiodun, B., Braconnot, P., Chou, S. C., Collins, W., Cox, P., Driouech, F., Emori, S., Eyring, V., Eyring, V., and Forest, C.: Evaluation of climate models, in: *Climate change 2013: the physical science basis. Contribution of Working Group I to the Fifth Assessment Report of the Intergovernmental Panel on Climate Change*, Cambridge University Press, 741–866, 2014.
- Forrest, M., Eronen, J. T., Utescher, T., Knorr, G., Stepanek, C., Lohmann, G., and Hickler, T.: Climate-vegetation modelling and fossil plant data suggest low atmospheric  $\text{CO}_2$  in the late Miocene, *Clim. Past*, 11, 1701–1732, <https://doi.org/10.5194/cp-11-1701-2015>, 2015.
- Forrest, M., Tost, H., Lelieveld, J., and Hickler, T.: Including vegetation dynamics in an atmospheric chemistry-enabled general circulation model: linking LPJ-GUESS (v4.0) with the EMAC modelling system (v2.53), *Geosci. Model Dev.*, 13, 1285–1309, <https://doi.org/10.5194/gmd-13-1285-2020>, 2020.
- Ganzeveld, L., Lelieveld, J., Dentener, F., Krol, M., Bouwman, A., and Roelofs, G.-J.: Global soil-biogenic  $\text{NO}_x$  emissions and the role of canopy processes, *J. Geophys. Res.-Atmos.*, 107, 4298, <https://doi.org/10.1029/2001JD001289>, 2002.
- Geron, C., Guenther, A., Greenberg, J., Karl, T., and Rasmussen, R.: Biogenic volatile organic compound emissions from desert vegetation of the southwestern US, *Atmos. Environ.*, 40, 1645–1660, 2006.
- Granier, C., Pétron, G., Müller, J.-F., and Brasseur, G.: The impact of natural and anthropogenic hydrocarbons on the tropospheric budget of carbon monoxide, *Atmos. Environ.*, 34, 5255–5270, 2000.
- Grote, R. and Niinemets, Ü.: Modeling volatile isoprenoid emissions – a story with split ends, *Plant Biol.*, 9, e42–e59, 2007.
- Guenther, A., Monson, R. K., and Fall, R.: Isoprene and monoterpene emission rate variability: observations with eucalyptus and emission rate algorithm development, *J. Geophys. Res.-Atmos.*, 96, 10799–10808, 1991.
- Guenther, A., Zimmerman, P. R., Harley, P. C., Monson, R. K., and Fall, R.: Isoprene and monoterpene emission rate variability: model evaluations and sensitivity analyses, *J. Geophys. Res.-Atmos.*, 98, 12609–12617, 1993.
- Guenther, A., Hewitt, C. N., Erickson, D., Fall, R., Geron, C., Graedel, T., Harley, P., Klinger, L., Lerdau, M., McKay, W., McKay, W. A., and Pierce, T.: A global model of natural volatile organic compound emissions, *J. Geophys. Res.-Atmos.*, 100, 8873–8892, <https://doi.org/10.1029/94JD02950>, 1995.
- Guenther, A., Archer, S., Greenberg, J., Harley, P., Helmig, D., Klinger, L., Vierling, L., Wildermuth, M., Zimmerman, P., and Zitzer, S.: Biogenic hydrocarbon emissions and landcover/climate change in a subtropical savanna, *Phys. Chem. Earth, Pt. B*, 24, 659–667, 1999.
- Guenther, A., Karl, T., Harley, P., Wiedinmyer, C., Palmer, P. I., and Geron, C.: Estimates of global terrestrial isoprene emissions using MEGAN (Model of Emissions of Gases and Aerosols from Nature), *Atmos. Chem. Phys.*, 6, 3181–3210, <https://doi.org/10.5194/acp-6-3181-2006>, 2006.
- Guenther, A. B., Jiang, X., Heald, C. L., Sakulyanontvittaya, T., Duhl, T., Emmons, L. K., and Wang, X.: The Model of Emissions of Gases and Aerosols from Nature version 2.1 (MEGAN2.1): an extended and updated framework for modeling biogenic emissions, *Geosci. Model Dev.*, 5, 1471–1492, <https://doi.org/10.5194/gmd-5-1471-2012>, 2012.
- Hantson, S., Knorr, W., Schurgers, G., Pugh, T. A., and Arneth, A.: Global isoprene and monoterpene emissions under changing climate, vegetation,  $\text{CO}_2$  and land use, *Atmos. Environ.*, 155, 35–45, 2017.
- Harley, P., Vasconcellos, P., Vierling, L., Pinheiro, C. C. D. S., Greenberg, J., Guenther, A., Klinger, L., Almeida, S. S. D., Neill, D., Baker, T., and Phillips, O.: Variation in potential for isoprene emissions among Neotropical forest sites, *Glob. Change Biol.*, 10, 630–650, 2004.
- Harrison, S. P., Morfopoulos, C., Dani, K. S., Prentice, I. C., Arneth, A., Atwell, B. J., Barkley, M. P., Leishman, M. R., Loreto, F., Medlyn, B. E., and Niinemets, Ü.: Volatile isoprenoid emissions from plastid to planet, *New Phytol.*, 197, 49–57, 2013.
- Heald, C. L., Wilkinson, M. J., Monson, R. K., Alo, C. A., Wang, G., and Guenther, A.: Response of isoprene emission to ambient  $\text{CO}_2$  changes and implications for global budgets, *Glob. Change Biol.*, 15, 1127–1140, 2009.
- Jöckel, P., Sander, R., Kerkweg, A., Tost, H., and Lelieveld, J.: Technical Note: The Modular Earth Submodel System (MESSy) – a new approach towards Earth System Modeling, *Atmos. Chem. Phys.*, 5, 433–444, <https://doi.org/10.5194/acp-5-433-2005>, 2005.
- Jöckel, P., Tost, H., Pozzer, A., Kunze, M., Kirner, O., Brenninkmeijer, C. A. M., Brinkop, S., Cai, D. S., Dyroff, C., Eckstein, J., Frank, F., Garny, H., Gottschaldt, K.-D., Graf, P., Grewe, V., Kerkweg, A., Kern, B., Matthes, S., Mertens, M., Meul, S., Neu-maier, M., Nützel, M., Oberländer-Hayn, S., Ruhnke, R., Runde, T., Sander, R., Scharffe, D., and Zahn, A.: Earth System Chemistry integrated Modelling (ESCiMo) with the Modular Earth Submodel System (MESSy) version 2.51, *Geosci. Model Dev.*, 9, 1153–1200, <https://doi.org/10.5194/gmd-9-1153-2016>, 2016.
- Jordan, C. F.: Derivation of leaf-area index from quality of light on the forest floor, *Ecology*, 50, 663–666, 1969.
- Karl, T., Guenther, A., Spirig, C., Hansel, A., and Fall, R.: Seasonal variation of biogenic VOC emissions above a mixed hardwood forest in northern Michigan, *Geophys. Res. Lett.*, 30, 2186, <https://doi.org/10.1029/2003GL018432>, 2003.
- Kerkweg, A., Sander, R., Tost, H., and Jöckel, P.: Technical note: Implementation of prescribed (OFFLEM), calculated (ONLEM), and pseudo-emissions (TNUDGE) of chemical species in the

- Modular Earth Submodel System (MESSy), *Atmos. Chem. Phys.*, 6, 3603–3609, <https://doi.org/10.5194/acp-6-3603-2006>, 2006.
- Kesselmeier, J. and Staudt, M.: Biogenic volatile organic compounds (VOC): an overview on emission, physiology and ecology, *J. Atmos. Chem.*, 33, 23–88, 1999.
- Lalic, B., Firanj, A., Mihailovic, D. T., and Podrascanin, Z.: Parameterization of PAR vertical profile within horizontally uniform forest canopies for use in environmental modeling, *J. Geophys. Res.-Atmos.*, 118, 8156–8165, 2013.
- Lamb, B., Westberg, H., Allwine, G., and Quarles, T.: Biogenic hydrocarbon emissions from deciduous and coniferous trees in the United States, *J. Geophys. Res.-Atmos.*, 90, 2380–2390, 1985.
- Lamb, B., Guenther, A., Gay, D., and Westberg, H.: A national inventory of biogenic hydrocarbon emissions, *Atmos. Environ.*, 21, 1695–1705, 1987.
- Lantz, A. T., Allman, J., Weraduwaage, S. M., and Sharkey, T. D.: Isoprene: New insights into the control of emission and mediation of stress tolerance by gene expression, *Plant Cell Environ.*, 42, 2808–2826, 2019.
- Laothawornkitkul, J., Paul, N. D., Vickers, C. E., Possell, M., Taylor, J. E., Mullineaux, P. M., and Hewitt, C. N.: Isoprene emissions influence herbivore feeding decisions, *Plant Cell Environ.*, 31, 1410–1415, 2008.
- Lathiere, J., Hauglustaine, D. A., De Noblet-Ducoudré, N., Krinner, G., and Folberth, G. A.: Past and future changes in biogenic volatile organic compound emissions simulated with a global dynamic vegetation model, *Geophys. Res. Lett.*, 32, L20818, <https://doi.org/10.1029/2005GL024164>, 2005.
- Lathière, J., Hauglustaine, D. A., Friend, A. D., De Noblet-Ducoudré, N., Viovy, N., and Folberth, G. A.: Impact of climate variability and land use changes on global biogenic volatile organic compound emissions, *Atmos. Chem. Phys.*, 6, 2129–2146, <https://doi.org/10.5194/acp-6-2129-2006>, 2006.
- Lelieveld, J., Crutzen, P. J., and Dentener, F. J.: Changing concentration, lifetime and climate forcing of atmospheric methane, *Tellus B*, 50, 128–150, 1998.
- Levis, S., Wiedinmyer, C., Bonan, G. B., and Guenther, A.: Simulating biogenic volatile organic compound emissions in the Community Climate System Model, *J. Geophys. Res.-Atmos.*, 108, 4659, <https://doi.org/10.1029/2002JD003203>, 2003.
- Mao, J. and Yan, B.: Global Monthly Mean Leaf Area Index Climatology, 1981–2015, ORNL DAAC [data set], <https://doi.org/10.3334/ORNLDAAAC/1653>, 2019.
- Naik, V., Delire, C., and Wuebbles, D. J.: Sensitivity of global biogenic isoprenoid emissions to climate variability and atmospheric CO<sub>2</sub>, *J. Geophys. Res.-Atmos.*, 109, D06301, <https://doi.org/10.1029/2003JD004236>, 2004.
- Niinemets, Ü.: Mild versus severe stress and BVOCs: thresholds, priming and consequences, *Trends Plant Sci.*, 15, 145–153, 2010.
- Niinemets, Ü., Tenhunen, J., Harley, P. C., and Steinbrecher, R.: A model of isoprene emission based on energetic requirements for isoprene synthesis and leaf photosynthetic properties for Liquidambar and Quercus, *Plant Cell Environ.*, 22, 1319–1335, 1999.
- Niinemets, Ü., Seufert, G., Steinbrecher, R., and Tenhunen, J. D.: A model coupling foliar monoterpene emissions to leaf photosynthetic characteristics in Mediterranean evergreen Quercus species, *New Phytol.*, 153, 257–275, 2002.
- Otter, L., Guenther, A., Wiedinmyer, C., Fleming, G., Harley, P., and Greenberg, J.: Spatial and temporal variations in biogenic volatile organic compound emissions for Africa south of the equator, *J. Geophys. Res.-Atmos.*, 108, 8505, <https://doi.org/10.1029/2002JD002609>, 2003.
- Pfister, G. G., Emmons, L. K., Hess, P. G., Lamarque, J. F., Orlando, J. J., Walters, S., Guenther, A., Palmer, P., and Lawrence, P. J.: Contribution of isoprene to chemical budgets: A model tracer study with the NCAR CTM MOZART-4, *J. Geophys. Res.-Atmos.*, 113, D05308, <https://doi.org/10.1029/2007JD008948>, 2008.
- Poisson, N., Kanakidou, M., and Crutzen, P. J.: Impact of non-methane hydrocarbons on tropospheric chemistry and the oxidizing power of the global troposphere: 3-dimensional modelling results, *J. Atmos. Chem.*, 36, 157–230, 2000.
- Pozzer, A., Reifenberg, S. F., Kumar, V., Franco, B., Kohl, M., Taraborrelli, D., Gromov, S., Ehrhart, S., Jöckel, P., Sander, R., Fall, V., Rosanka, S., Karydis, V., Akritidis, D., Emmerichs, T., Crippa, M., Guizzardi, D., Kaiser, J. W., Clarisse, L., Kiendler-Scharr, A., Tost, H., and Tsimpidi, A.: Simulation of organics in the atmosphere: evaluation of EMACv2.54 with the Mainz Organic Mechanism (MOM) coupled to the ORACLE (v1.0) submodel, *Geosci. Model Dev.*, 15, 2673–2710, <https://doi.org/10.5194/gmd-15-2673-2022>, 2022.
- Rap, A., Scott, C. E., Spracklen, D. V., Bellouin, N., Forster, P. M., Carslaw, K. S., Schmidt, A., and Mann, G.: Natural aerosol direct and indirect radiative effects, *Geophys. Res. Lett.*, 40, 3297–3301, 2013.
- Roeckner, E., Brokopf, R., Esch, M., Giorgetta, M., Hagemann, S., Kornblüeh, L., Manzini, E., Schlese, U., and Schulzweida, U.: Sensitivity of simulated climate to horizontal and vertical resolution in the ECHAM5 atmosphere model, *J. Climate*, 19, 3771–3791, 2006.
- Rybka, H. and Tost, H.: Uncertainties in future climate predictions due to convection parameterisations, *Atmos. Chem. Phys.*, 14, 5561–5576, <https://doi.org/10.5194/acp-14-5561-2014>, 2014.
- Sanderson, M. G., Jones, C. D., Collins, W. J., Johnson, C. E., and Derwent, R. G.: Effect of climate change on isoprene emissions and surface ozone levels, *Geophys. Res. Lett.*, 30, 1936, <https://doi.org/10.1029/2003GL017642>, 2003.
- Schurgers, G., Arneth, A., Holzinger, R., and Goldstein, A. H.: Process-based modelling of biogenic monoterpene emissions combining production and release from storage, *Atmos. Chem. Phys.*, 9, 3409–3423, <https://doi.org/10.5194/acp-9-3409-2009>, 2009.
- Scott, C. E., Rap, A., Spracklen, D. V., Forster, P. M., Carslaw, K. S., Mann, G. W., Pringle, K. J., Kivekäs, N., Kulmala, M., Lihavainen, H., and Tunved, P.: The direct and indirect radiative effects of biogenic secondary organic aerosol, *Atmos. Chem. Phys.*, 14, 447–470, <https://doi.org/10.5194/acp-14-447-2014>, 2014.
- Sharkey, T. D., Wiberley, A. E., and Donohue, A. R.: Isoprene emission from plants: why and how, *Annals of Botany*, 101, 5–18, 2008.
- Shim, C., Wang, Y., Choi, Y., Palmer, P. I., Abbot, D. S., and Chance, K.: Constraining global isoprene emissions with Global Ozone Monitoring Experiment (GOME) formaldehyde column measurements, *J. Geophys. Res.-Atmos.*, 110, D24301, <https://doi.org/10.1029/2004JD005629>, 2005.

- Sindelarova, K., Granier, C., Bouarar, I., Guenther, A., Tilmes, S., Stavrou, T., Müller, J.-F., Kuhn, U., Stefani, P., and Knorr, W.: Global data set of biogenic VOC emissions calculated by the MEGAN model over the last 30 years, *Atmos. Chem. Phys.*, 14, 9317–9341, <https://doi.org/10.5194/acp-14-9317-2014>, 2014.
- Sitch, S., Smith, B., Prentice, I. C., Arneth, A., Bondeau, A., Cramer, W., Kaplan, J. O., Levis, S., Lucht, W., Sykes, M. T., and Thonicke, K.: Evaluation of ecosystem dynamics, plant geography and terrestrial carbon cycling in the LPJ dynamic global vegetation model, *Glob. Change Biol.*, 9, 161–185, <https://doi.org/10.1046/j.1365-2486.2003.00569.x>, 2003.
- Smith, B., Prentice, I. C., and Sykes, M. T.: Representation of vegetation dynamics in the modelling of terrestrial ecosystems: comparing two contrasting approaches within European climate space, *Global Ecol. Biogeogr.*, 10, 621–637, <https://doi.org/10.1046/j.1466-822X.2001.t01-1-00256.x>, 2001.
- Smith, B., Wårlind, D., Arneth, A., Hickler, T., Leadley, P., Silberg, J., and Zaehle, S.: Implications of incorporating N cycling and N limitations on primary production in an individual-based dynamic vegetation model, *Biogeosciences*, 11, 2027–2054, <https://doi.org/10.5194/bg-11-2027-2014>, 2014.
- Sporre, M. K., Blichner, S. M., Karset, I. H. H., Makkonen, R., and Berntsen, T. K.: BVOC–aerosol–climate feedbacks investigated using NorESM, *Atmos. Chem. Phys.*, 19, 4763–4782, <https://doi.org/10.5194/acp-19-4763-2019>, 2019.
- Sun, G., Caldwell, P. V., and McNulty, S. G.: Modelling the potential role of forest thinning in maintaining water supplies under a changing climate across the conterminous United States, *Hydrol. Process.*, 29, 5016–5030, 2015.
- Sun, Z., Hüve, K., Vislap, V., and Niinemets, Ü.: Elevated [CO<sub>2</sub>] magnifies isoprene emissions under heat and improves thermal resistance in hybrid aspen, *J. Exp. Bot.*, 64, 5509–5523, 2013.
- Taylor, T. C., McMahon, S. M., Smith, M. N., Boyle, B., Völle, C., van Haren, J., Simova, I., Meir, P., Ferreira, L. V., de Camargo, P. B., and da Costa, A. C.: Isoprene emission structures tropical tree biogeography and community assembly responses to climate, *New Phytol.*, 220, 435–446, <https://doi.org/10.1111/nph.15304>, 2018.
- Tingey, D. T., Manning, M., Grothaus, L. C., and Burns, W. F.: Influence of light and temperature on monoterpene emission rates from slash pine, *Plant Physiol.*, 65, 797–801, 1980.
- Tingey, D. T., Evans, R., and Gumpertz, M.: Effects of environmental conditions on isoprene emission from live oak, *Planta*, 152, 565–570, 1981.
- Tost, H.: Chemistry–climate interactions of aerosol nitrate from lightning, *Atmos. Chem. Phys.*, 17, 1125–1142, <https://doi.org/10.5194/acp-17-1125-2017>, 2017.
- Vella, R., Forrest, M., Lelieveld, J., and Tost, H.: MESSy-vella-et al-gmd-2022-154 (EMAC (v2.55), LPJ-GUESS (v4.0)), Zenodo [code], <https://doi.org/10.5281/zenodo.6772205>, 2022.
- Wang, B., Shugart, H. H., and Lerdau, M. T.: Complexities between plants and the atmosphere, *Nat. Geosci.*, 12, 693–694, 2019.
- Weiss, A. and Norman, J.: Partitioning solar radiation into direct and diffuse, visible and near-infrared components, *Agr. Forest Meteorol.*, 34, 205–213, 1985.
- Weiss, M., Miller, P. A., van den Hurk, B. J., van Noije, T., Ștefănescu, S., Haarsma, R., Van Ulft, L. H., Hazeleger, W., Le Sager, P., Smith, B., and Schurgers, G.: Contribution of dynamic vegetation phenology to decadal climate predictability, *J. Climate*, 27, 8563–8577, <https://doi.org/10.1175/JCLI-D-13-00684.1>, 2014.
- Westberg, H., Lamb, B., Kempf, K., and Allwine, G.: Isoprene emission inventory for the BOREAS southern study area, *Tree Physiol.*, 20, 735–743, 2000.
- Zuo, Z., Weraduwage, S. M., Lantz, A. T., Sanchez, L. M., Weise, S. E., Wang, J., Childs, K. L., and Sharkey, T. D.: Isoprene acts as a signaling molecule in gene networks important for stress responses and plant growth, *Plant Physiol.*, 180, 124–152, 2019.